

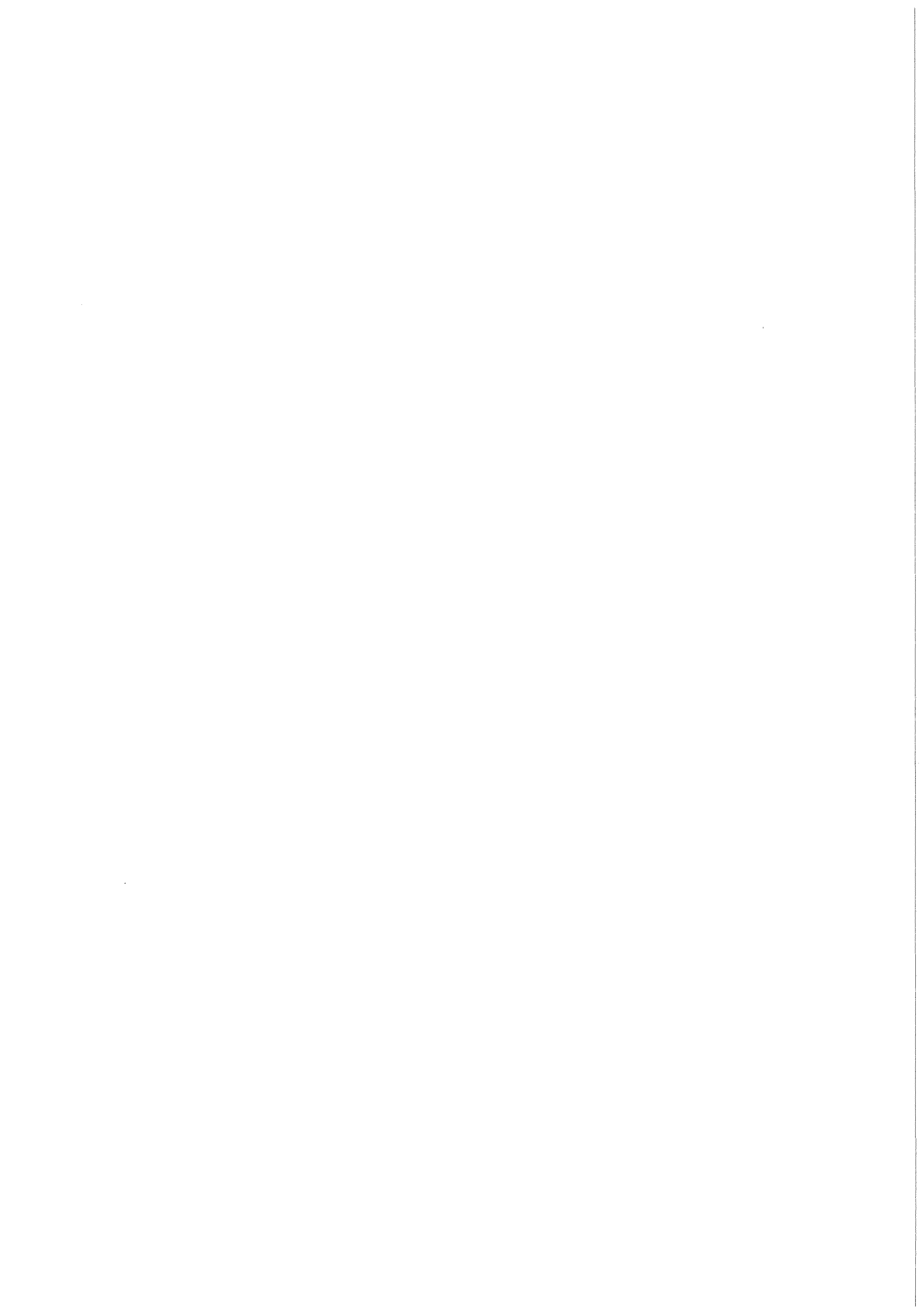
KfK 3507  
August 1983

**Temperature Escalation  
in PWR Fuel Rod Simulators due  
to the Zircaloy/Steam Reaction:  
Tests ESSI-1,2,3  
Test Results Report**

S. Hagen, H. Malauschek, K. P. Wallenfels  
S. O. Peck

Hauptabteilung Ingenieurtechnik  
Projekt Nukleare Sicherheit

**Kernforschungszentrum Karlsruhe**



KERNFORSCHUNGSZENTRUM KARLSRUHE  
HAUPTABTEILUNG INGENIEURTECHNIK  
PROJEKT NUKLEARE SICHERHEIT

KfK 3507

Temperature Escalation in PWR Fuel Rod Simulators  
due to the Zircaloy/Steam Reaction: Tests ESSI-1,2,3.

Test Results Report

S. Hagen, H. Malauschek, K.P. Wallenfels, S.O. Peck<sup>+</sup>)

<sup>+</sup>) USNRC Delegate to Kernforschungszentrum Karlsruhe  
from EG&G, Idaho Falls, Idaho.

KERNFORSCHUNGSZENTRUM KARLSRUHE GMBH, KARLSRUHE

Als Manuskript vervielfältigt  
Für diesen Bericht behalten wir uns alle Rechte vor

Kernforschungszentrum Karlsruhe GmbH  
ISSN 0303-4003

## Summary

This report discusses the test conduct, results, and posttest appearance of three scoping tests (ESSI-1,2,3) investigating temperature escalation in zircaloy clad fuel rods. The experiments are part of an out-of-pile program using electrically heated fuel rod simulators to investigate PWR fuel element behavior up to temperatures of 2000°C. These experiments are part of the PNS Severe Fuel Damage Program. The temperature escalation is caused by the exothermal zircaloy/steam reaction, whose reaction rate increases exponentially with the temperature. The tests were performed using different initial oxide layers as a major parameter, obtained by varying the heatup rates and steam exposure times.

In every test, a temperature escalation was observed. The maximum rod surface temperature never exceeded 2200°C. The escalation began in the upper region of the rods and moved down the rods towards the lower end, opposite to the direction of steam flow. For fast initial heatup rates the runoff of molten zircaloy was a limiting process for the escalation. For slow heatup rates the formation of a protective oxide layer reduced the reaction rate.

The posttest appearance of the fuel rod simulators showed that at slow heatup rates oxidation of the cladding was complete, and the fuel rod was relatively intact. Conversely, at fast heatup rates, relatively little oxidation, extensive dissolution of the UO<sub>2</sub> pellets, and runoff of molten cladding were observed.

Temperatur Eskalation in DWR Brennstabsimulatoren infolge der Zirkaloy/Dampf Reaktion: Versuche ESSI 1, 2, 3; Versuchsergebnisse.

---

### Kurzfassung

Dieser KfK-Bericht beschreibt die Versuchsdurchführung und die Ergebnisse der ersten drei Übersichtsversuche einer Serie zur Untersuchung der Temperatureskalation von zirkaloyumhüllten Brennstäben. Diese Serie gehört zu den Out-of-pile Experimenten mit elektrisch beheizten Brennstabsimulatoren, die das DWR Brennelementverhalten im Temperaturbereich bis 2000°C untersuchen sollen. Die Experimente werden im Rahmen des PNS Severe Fuel Damage Programms durchgeführt.

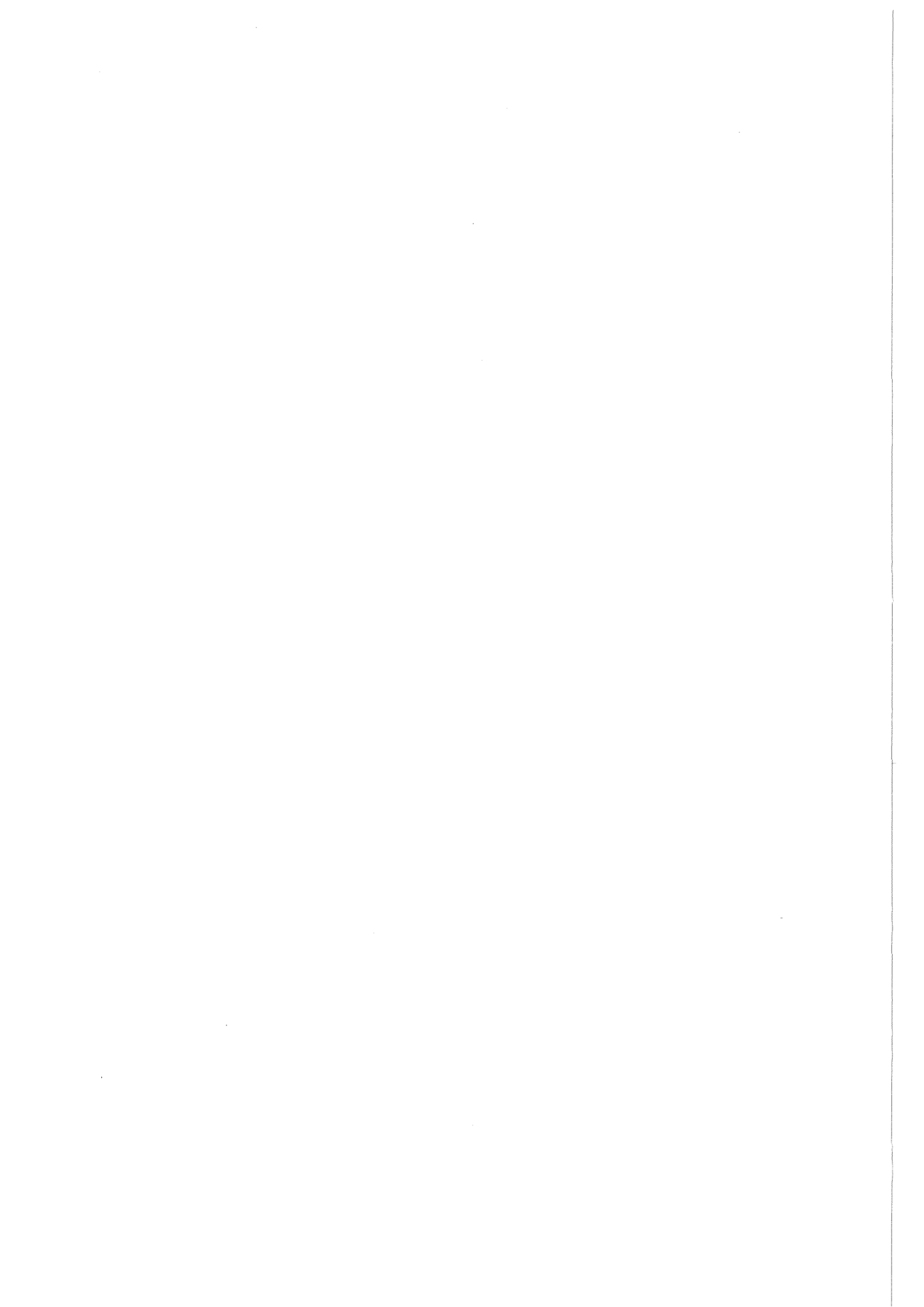
Die Temperatureskalation wird durch die exotherme Zirkon-Wasserdampf-Reaktion hervorgerufen. Die Stärke dieser Reaktion nimmt exponentiell mit der Temperatur zu. Bei den Versuchen wurde die anfängliche Oxidschicht zum Beginn der Eskalation variiert. Dies wurde durch Aufheizen in Argon und schnelles oder langsames Aufheizen in Dampf erreicht.

Bei allen Versuchen stellte sich eine Eskalation der Temperatur ein. Die maximal erreichte Temperatur betrug etwa 2200°C. Die Eskalation begann im oberen Bereich des Stabes und setzte sich nach unten hin fort. Dies ist entgegengesetzt zur Richtung der Dampfströmung. Für eine schnelle anfängliche Anstiegsrate stellt das Abfließen des geschmolzenen Zirkaloy aus dem Reaktionsbereich eine inhärente Beschränkung der Eskalation dar. Bei langsamen anfänglichem Temperaturanstieg wird die Eskalation durch den Aufbau der festhaftenden, den Sauerstofffluß verlangsamen Oxidschicht, beschränkt.

Das Aussehen des Bündels nach dem Versuch zeigte, daß beim langsamen Aufheizen die Zirkaloy-Hülle vollkommen oxidiert war. Der Brennstabsimulator hat seine ursprüngliche Form beibehalten. Beim schnellen anfänglichen Aufheizen war nur eine dünne Oxidschicht entstanden und das geschmolzene Zirkaloy hatte UO<sub>2</sub> aufgelöst. Die entstandene Schmelze ist heruntergelaufen.

Contents

	Page
Introduction	3
Experiment facility	5
Test conduct	
ESSI-1	6
ESSI-2	7
ESSI-3	8
General results	8
Specific results for ESSI-1	9
Specific results for ESSI-2	11
Specific results for ESSI-3	12
Acknowledgements	13
References	13
List of figures and tables	14





## Introduction

Project Nuclear Safety (PNS) is sponsoring an extensive Severe Fuel Damage Program at the Nuclear Research Center Karlsruhe (KFK). Part of these investigations are out-of-pile experiments with electrically heated fuel rod simulators (CORA Program). These experiments will investigate mechanisms damaging PWR fuel elements at temperatures up to 2000°C.

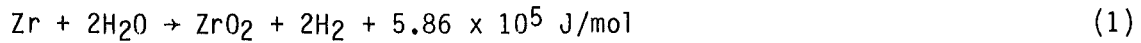
The construction of the CORA facility is under way. CORA will permit experiments to be performed under as realistic as possible conditions. For that part of the out-of-pile program that does not require the special features of the CORA facility, experiments are being performed in the NIELS facility. A series of single rod and bundle experiments investigating temperature escalation due to the exothermal zirconium/steam reaction have been conducted. This report describes three single rod scoping tests on escalation behavior.

The reason for starting the SFD out-of-pile tests with experiments on the escalation behavior is twofold:

1. The main parameter for SFD fuel rod behavior is the degree of oxidation: The amount of dissolution of UO<sub>2</sub> by zircaloy on one hand, and the fragmentation of the fuel rod on the other hand, depend decisively on the oxidation. The degree of oxidation depends on the temperature rise rate, which may be dominated by the escalation.
2. Inpile bundle experiments on Severe Fuel Damage are now being conducted by EG&G in the Power Burst Facility at the Idaho National Engineering Laboratory. In the tests a 32 rod bundle (6x6 without the corner rods) surrounded by a zircaloy shroud is heated in a steam atmosphere. Preliminary temperature calculations, which did not take into account any limiting effects (e.g. zircaloy runoff) predicted temperatures due to the escalation of over 3000°C.

Therefore, it was necessary to obtain experimental data about the potential temperature escalation of zircaloy clad fuel rods in order to evaluate the CORA and PBF experiments.

The oxidation of zirconium in steam is an exothermic reaction which can be expressed as:



In the energy balance  $10.7 \times 10^5 \text{ J/mol}$  are gained by the formation of the oxide and  $4.80 \times 10^5 \text{ J/mol}$  lost by the dissociation of the two moles of  $\text{H}_2\text{O}$ . The energy potential of this reaction is remarkable. The complete oxidation of a 10.75 mm zircaloy cladding (1.5 gm/cm length) in steam would deliver an energy of 9600 J/cm. Under adiabatic conditions this energy is sufficient to heat the cladding and fuel to  $3700^\circ\text{C}$ , including the melting of both materials.

Zirconium forms a protective layer as it oxidizes. The reaction is therefore controlled by the diffusion of oxygen through the oxide, and the reaction rate is inversely proportional to the oxide thickness.

$$\frac{dW}{dt} = K \frac{1}{W} \quad (2)$$

where

$W$  = kinetic parameter (oxygen uptake per unit surface area ( $\text{kg/m}^2$ ), metal reacted per unit surface area ( $\text{kg/m}^2$ ), or oxide thickness (m)), and  
 $t$  = time (s).

The proportionality constant  $K$  has been observed to be an Arrhenius function of temperature, so that

$$K = A \exp(-B/RT) \quad (3)$$

where

$A, B$  = constants to be determined experimentally, and

$T$  = temperature of cladding (K).

Integrating equation (2) for an initial condition of zero oxide at zero time gives

$$W^2 = 2 A \exp (-B/RT)t \quad (4)$$

which is known as a parabolic rate equation. If the heat generated by the reaction can be removed from the system so that the cladding temperature remains constant, the rate of reaction will decline as  $1/W$ . If the heat cannot be removed, or cannot be removed fast enough, and the cladding temperature rises, the exponential dependence of the reaction rate on temperature may dominate the reaction and give rise to a rapid temperature escalation. The cladding behavior will then be determined by the system boundary conditions (heat removal) and such processes that may inherently limit the heat generated in the cladding.

Inherent limitations to the heat gain include: (a) zircaloy consumption, (b) removal of zircaloy from the reaction, such as by molten runoff, (c) steam starvation, and (d) hydrogen blanketing. The heat losses will depend on the system temperature, configuration, and available coolant. The modes of heat transport will include radiation, convection and conduction, the relative importance of which will depend on the current state of the rod and boundary conditions.

### Experiment Facility

The tests were performed in the NIELS facility located in the Hauptabteilung Ingenieurtechnik at KfK. Figures 1 and 2 show side and top cross sections of the fuel rod simulators, shroud, and insulation. The fuel rod simulators conformed as nearly as possible to German PWR dimensions, using zircaloy cladding of 10.75 mm outer and 9.29 mm inner diameter, UO<sub>2</sub> ring pellets of 9.2 mm outer and 6.1 mm inner diameter, and tungsten heater rods of 6.0 mm diameter. The overall length of the simulators was 250 mm.

To simulate the exothermal reaction energy of neighboring rods a zircaloy shroud was installed around the fuel rod simulators. The shroud had an inner diameter of 26.5 mm and an 0.5 mm thick wall.

To inhibit radial heat losses the simulator and shroud were surrounded by 100 mm of fiber ceramic insulation as shown in Figure 3. The inner 25 mm was made from  $ZrO_2$  and the outer 75 mm from an  $Al_2O_3/SiO_2$  mixture. The  $ZrO_2$  fiberboard is 92% porous and has a thermal conductivity of 0.24 W/m-K at 1650°C. The  $Al_2O_3/SiO_2$  mixture has a conductivity of 0.20 W/m-K at 1100°C. At full power to the simulators the radial losses were estimated to be less than 10% of the input power.

Steam was inlet to the shroud through the double tube system shown in Figures 1 and 2. The four holes in this system ensured a uniform supply of steam to the surface of the rod.

Temperatures on the surfaces of the rod and shroud were measured by two color pyrometers. Holes for the measurement were cut into the shroud and insulation 140 mm above the lower end of the rod. Temperatures in the insulation were measured by Ni-Cr/Ni thermocouples with Inconel sheaths. The measuring positions were 12 mm from the inner, and 12 mm from the outer surface of the insulation at elevations of 140 mm and 130 mm above the lower end of the rod.

## Test Conduct

### ESSI-1

A major parameter of the three scoping tests was to investigate the degree of escalation corresponding to different initial oxide layers. Test ESSI-1 was intended to have a minimum initial oxide thickness and thus the rod was heated in argon until the surface temperature reached about 1700°C before steam was introduced. During the same time the shroud had reached a temperature of about 1200°C by radiant heating from the rod.

Figure 4 shows the controlled electric voltage (V), the resulting current (I), and the calculated resistance ( $V/I$ ) and power ( $V \times I$ ) for ESSI-1. The voltage was raised by steps every 3 minutes and then held constant. The current followed the voltage increase at each step increase but then decreased during the hold periods due to the increasing resistance of the heater, which was caused by the increasing temperature. The current decrease is responsible for the power decrease during each hold period.

The last step increase in voltage was made at approximately 24 minutes, after which the system was allowed to come to equilibrium. At about 32 minutes steam (32 g/min) was introduced. The rod temperature increase due to the zircaloy/steam reaction increased the rod resistance which caused a decreased current and input power. After the reaction stopped, steam cooling significantly lowered the rod temperature, decreasing the resistivity and thus increasing the input current and power. The voltage was held constant throughout. At approximately 35 minutes the power supply was shut off. Table 1 gives the measured voltage and current, and calculated resistance and power for ESSI-1.

#### ESSI-2

The objective of test ESSI-2 was an initial heatup rate of roughly  $4^{\circ}\text{C/s}$  in a continuous steam flow (23 g/min). As shown in Figure 5 the voltage was increased linearly with the exception of three hold periods, the last being the final test voltage. The first two hold periods were used to recalibrate the two-color pyrometer. In each of these hold periods a behavior similar to that of ESSI-1 was observed in that the current decreased as the rod temperature and resistance increased. In the third period at constant voltage a sudden increase in current was observed. This is thought to have been due to the movement of molten zircaloy causing a short circuit for the electric current through the rod. The effect did not last very long as the current immediately decreased following the overall temperature increase of the rod. Table 2 gives the measured voltage and current, and calculated resistance and power for ESSI-2.

### ESSI-3

The objective of test ESSI-3 was a slow initial heatup rate of  $0.5^{\circ}\text{C}/\text{s}$  in a steam atmosphere (17 g/min) in order to produce a thick oxide layer before the escalation began. The voltage was increased linearly throughout the test. Just after 40 minutes the rod temperature escalated producing the small change in current shown in Figure 6. There is no explanation for the current change at 35 minutes. Table 3 gives the measured voltage and current, and calculated resistance and power for ESSI-3.

In Figure 7 the graphs from ESSI-1 and ESSI-3 are compared. Neglecting the steps in ESSI-1 the voltage rise is roughly the same for the two experiments. The reduced cooling capability of the argon used for ESSI-1 results in a higher temperature, producing a higher resistance.

### General Results

Figures 8 through 10 show the pyrometer measured surface temperatures on the rod and shroud, and the thermocouple measured temperatures near (1 cm depth) the inner and outer surfaces of the insulation compared to the electric power input for tests ESSI-1 through 3, respectively. The rod surface temperature for ESSI-3 is suspect, since the window through which the pyrometer measurement was made was covered by a deposit. Figures 11 through 13 show the temperatures measured in the insulation and electric power over an extended time scale.

In each test the exothermal zircaloy/steam reaction together with the insulated surroundings led to a temperature escalation on the rod and shroud. The maximum temperature reached was about  $2200^{\circ}\text{C}$  on ESSI-1. In general, the escalation began at a lower temperature for the faster initial heatup rates. In each test the escalation began on the rods first, then began later on the shrouds. At the end of the tests the shroud temperatures were higher than the rod temperatures. Figure 14 compares the measured rod surface temperatures from each test and Figure 15 the measured shroud surface temperatures.

In order to compare the relative contributions of the zircaloy/steam reaction and the electric input power to the total power, the MULTRAN /1/ program was used to estimate the power generated in the rod and shroud of each test. MULTRAN is a modification of SIMTRAN, and solves the oxygen diffusion equations. The measured rod and shroud temperature as a function of time were input to the code. The posttest appearance of the shroud indicated that two sided oxidation should be used for the shroud calculations. Using the heat of reaction ( $5.86 \times 10^5$  J/mol-Zr) and an assumed reacting length of 10 cm, the zircaloy reaction powers were calculated. Figure 16 illustrates the calculated reaction powers for rod and shroud compared to electric input power for each test. Figure 17 shows the integrated power for each rod and shroud as a function of time. Figure 16 clearly shows that the reaction power during the escalation was greater than the input electric power. In addition, the power contributed by the shrouds was greater than the rods due to larger surface area and mass.

#### Specific Results for ESSI-1

Figure 8 shows a rod surface temperature of about 1700°C and a shroud surface temperature of just over 1200°C prior to the introduction of steam. These temperatures corresponded to an electric power of almost 1200 watts. After the steam was inlet (32 g/min) the rod reached a maximum of about 2200°C within 2 seconds, and the shroud a maximum of about 2100°C within 18 seconds. Note that compared to an initial temperature of 1200°C the shroud temperature rise was greater than that of the rod, and the subsequent decay slower. The heat production that caused the escalation was estimated by MULTRAN at 5 to 8 times the electric power input.

Steam consumption was estimated by the MULTRAN program from the input temperature time history using conservative Cathcart-Pawel oxidation kinetics. The maximum calculated oxygen consumption was 6 mg/cm<sup>2</sup>-s on the rod and 2.1 mg/cm<sup>2</sup>-s on the shroud. The cold steam inlet temperature (120°) and water cooling of the copper electrodes limited the hot region of the rod to about 10 cm in length. Using this assumption the above

estimated maximum oxygen consumption rates correspond to maximum steam consumption rates of 14 g H<sub>2</sub>O/min and 11 g H<sub>2</sub>O/min on the rod and shroud, respectively. Compared to the steam supply rate of 32 g/min the volume of hydrogen generated by the reaction could have been a significant fraction of the coolant. Experiments by Chung /2/ at Argonne National Laboratory have shown that at high hydrogen concentrations oxidation is diminished. It should be emphasized, however, that these calculations are intended to show order of magnitude effects.

Figure 18 shows the posttest appearance of the ESSI-1 rod. The axial temperature profile can be seen in the metallic appearance of the lower 6 cm and the increasingly oxidized upper rod. At about 13 cm above the bottom of the rod molten material has broken through and run down the outside. Most of the material refroze on the rod although some dropped down and refroze on the copper electrode and steam supply system. Apparently a significant amount of zircaloy has melted and runoff which may have limited the reaction with steam.

Figure 19 shows the posttest appearance of the ESSI-1 shroud. The same strong axial temperature profile is evident. Figures 27 and 28 show the shroud after dismantling. Only a thin oxide layer has formed at the inner surface of the shroud.

Details of the rod appearance are shown in Figure 20. The three pictures on the left show the upper portion of the rod while the right picture details the refrozen melt. Only a thin oxide layer has formed on the rod. By comparison with the 6 mm tungsten heater and 1.55 mm pellet thickness, the oxide layer can be estimated to be between 0.1 and 0.2 mm thick. A fully oxidized cladding would be approximately 1 mm thick. The remaining zircaloy has melted and run down the rod, much of it exiting through the crack in the righthand photograph. Most of the pellets have remained in place, glued together by the refrozen melt. Some melt has also refrozen within the rod. The deformation of the oxide layer indicates that, although brittle at room temperature, the oxide is surprisingly ductile at high temperature.



### Specific Results for ESSI-2

As shown in Figure 9 the temperature escalation of ESSI-2 began around 1100°C on the rod and reached a peak of about 2100°C. The shroud escalation began a little later and reached a peak of about 2050°C. As the peak temperatures were reached the escalation occurred very quickly. However, in contrast to ESSI-1 the high temperatures lasted over a minute and then decreased slowly. The electric power at the onset of escalation was around 2200 watts, or nearly twice that of ESSI-1. The MULTRAN calculated reaction power was less than the electric power (Figure 16) although the total reaction generated heat was greater than that of ESSI-1. The steam flow was continuous throughout the test at 23 g/min.

The maximum steam consumption rate as estimated by MULTRAN was 2.5 g H<sub>2</sub>O/min on the rod and 10 g H<sub>2</sub>O/min on the shroud. Steam starvation therefore did not occur although hydrogen reduced oxidation may have been important at the maximum consumption rate. Figure 21 shows the ESSI-1 rod posttest after removal of the shroud and before disassembly of the test rig. The metallic appearance of the lower 4 cm of the rod changing to severely oxidized cladding higher up shows the effect of the axial temperature profile. From 7.5 to 10.5 cm above the bottom of the rod the oxide has broken away revealing the smooth surface of refrozen material. The oxide layer most likely covered the rod during the high temperature portion of the transient and broke away during cooldown. In the right most photograph molten material which broke through the oxide and ran down is apparent. Figures 23 and 24 show details of these effects. The molten zircaloy has primarily run down in the gap between oxide and remaining fuel pellet. The left hand photograph of Figure 23 shows oxide that has partially adhered to the fuel pellet via refrozen melt. The maximum oxide layer thickness is estimated to be 0.3 mm. The two hold periods during heatup to readjust the pyrometers certainly influenced the oxide thickness.

The ESSI-2 shroud is shown in position in Figure 22, and after dismantling in Figures 27 and 29. The axial temperature profile effects are again obvious. The brittle nature of the shroud and two-sided oxidation are evident in Figure 29.

### Specific results for ESSI-3

Figure 10 shows the temperatures for ESSI-3. As discussed earlier, the temperature shown for the rod is suspect due to a fogged window. The electric power input was about 2400 watts at the onset of escalation, twice as much as for ESSI-1. Due to the slow initial heatup rate a substantial oxide layer had already formed when the escalation began. Nevertheless, the shroud reached a peak temperature of 1800°C. The MULTRAN calculated reaction heat generation rate for the shroud was less than the input electric power, although a small contribution to the overall power was calculated as early as 15 minutes before the escalation began.

The posttest appearance of the ESSI-3 rod is shown in figure 25. The axial temperature profile is clear from the oxide appearance. The upper portion of the rod is covered by a thick oxide layer. No broken pieces of oxide or molten zircaloy are apparent. The rod did not break during the entire posttest handling process.

The posttest appearance of the shroud is shown in figures 26, 27 and 30. As in ESSI-2, the shroud was very brittle and showed evidence of two-sided oxidation.

Acknowledgements

We thank Mr. A Grünhagen for the calculations with the MULTRAN Program.  
Thanks are due to Mrs. Ivanitsch for the careful typing of the manuscript.

References

- /1/ S. Malang,  
Jahresbericht PNS 1981; KfK 3250, S. 4200-2.
  
- /2/ H.M. Chung and G.R. Thomas  
"Rate-Limiting Effects of Gaseous Hydrogen on Zircaloy Oxidation"  
Proc. NRC Workshop: Impact of Hydrogen on Water Reactor Safety,  
Albuquerque, NM., January 26-28, 1981.

List of Figures and Tables

- Fig. 1: Sideview of the Experimental Arrangement for Tests ESSI-1,2,3.
- Fig. 2: Topview of the Experimental Arrangement for Tests ESSI-1,2,3.
- Fig. 3: Fiber Ceramic Insulation.
- Fig. 4: Voltage (V), Current (I), Resistance (R) and Electric Power (E) for Test ESSI-1.
- Fig. 5: Voltage (V), Current (I), Resistance (R) and Electric Power (E) for Test ESSI-2.
- Fig. 6: Voltage (V), Current (I), Resistance (R) and Electric Power (E) for Test ESSI-3.
- Fig. 7: Comparison of the Voltage (V), Currents (I), Resistances (R) and Electric Powers (E) for ESSI-1 and 3.
- Fig. 8: Temperature of the Fuel Rod Simulator (F), Shroud (S), and Insulation (I1,I2) compared to the Electric Power Input (E) for ESSI-1.
- Fig. 9: Temperature of the Fuel Rod Simulator (F), Shroud (S) and Insulation (I1,I2) compared to the Electric Power Input (E) for ESSI-2.
- Fig. 10: Temperature of the Fuel Rod Simulator (F), Shroud (S), and Insulation (I1,I2) compared to the Electric Power Input (E) for ESSI-3.
- Fig. 11: Temperatures 1 cm from the inner Surface (I1) and 1 cm from the outer Surface (I2) of the Insulation compared to Electric Power (E) for ESSI-1.
- Fig. 12: Temperatures 1 cm from the inner Surface (I1) and 1 cm from the outer Surface (I2) of the Insulation compared to Electric Power (E) for ESSI-2.
- Fig. 13: Temperatures 1 cm from the inner Surface (I1) and 1 cm from the outer Surface (I2) of the Insulation compared to Electric Power (E) for ESSI-3.
- Fig. 14: Comparison of Fuel Rod Simulator Temperatures for ESSI-1,2,3.
- Fig. 15: Comparison of Shroud Temperatures for ESSI-1,2,3.
- Fig. 16: Comparison of the MULTRAN calculated Reaction Powers for the Rods (HR) and Shrouds (HT) with the Electric Input Powers of ESSI-1,2,3.

- Fig. 17: Comparison of the MULTRAN calculated total Oxidation Generated Energy as a Function of time for ESSI-1,2,3.
- Fig. 18: Posttest Appearance of the ESSI-1 Fuel Rod Simulator shown from four Orientations.
- Fig. 19: Posttest Appearance of the ESSI-1 Shroud shown from four Orientations.
- Fig. 20: Details of the Fuel Rod Simulator Posttest Appearance for ESSI-1.
- Fig. 21: Posttest Appearance of the ESSI-2 Fuel Rod Simulator shown from four Orientations.
- Fig. 22: Posttest Appearance of the ESSI-2 Shroud shown from four Orientations.
- Fig. 23: Details of the Fuel Rod Simulator Posttest Appearance for ESSI-2.
- Fig. 24: Details of the Fuel Rod Simulator Posttest Appearance for ESSI-2.
- Fig. 25: Posttest Appearance of the ESSI-3 Fuel Rod Simulator shown from four Orientations.
- Fig. 26: Posttest Appearance of the ESSI-3 Shroud shown from four Orientations.
- Fig. 27: Fuel Rod Simulators and Shrouds from Tests ESSI-1,2,3 after Dismantling.
- Fig. 28: Upper Part of Shroud from ESSI-1 after Dismantling.
- Fig. 29: Upper Part of Shroud from ESSI-2 after Dismantling.
- Fig. 30: Upper Part of Shroud from ESSI-3 after Dismantling.
- 
- Tab. 1: Voltage, Current, Power and Resistance for Test ESSI-1
- Tab. 2: Voltage, Current, Power and Resistance for Test ESSI-2
- Tab. 3: Voltage, Current, Power and Resistance for Test ESSI-3

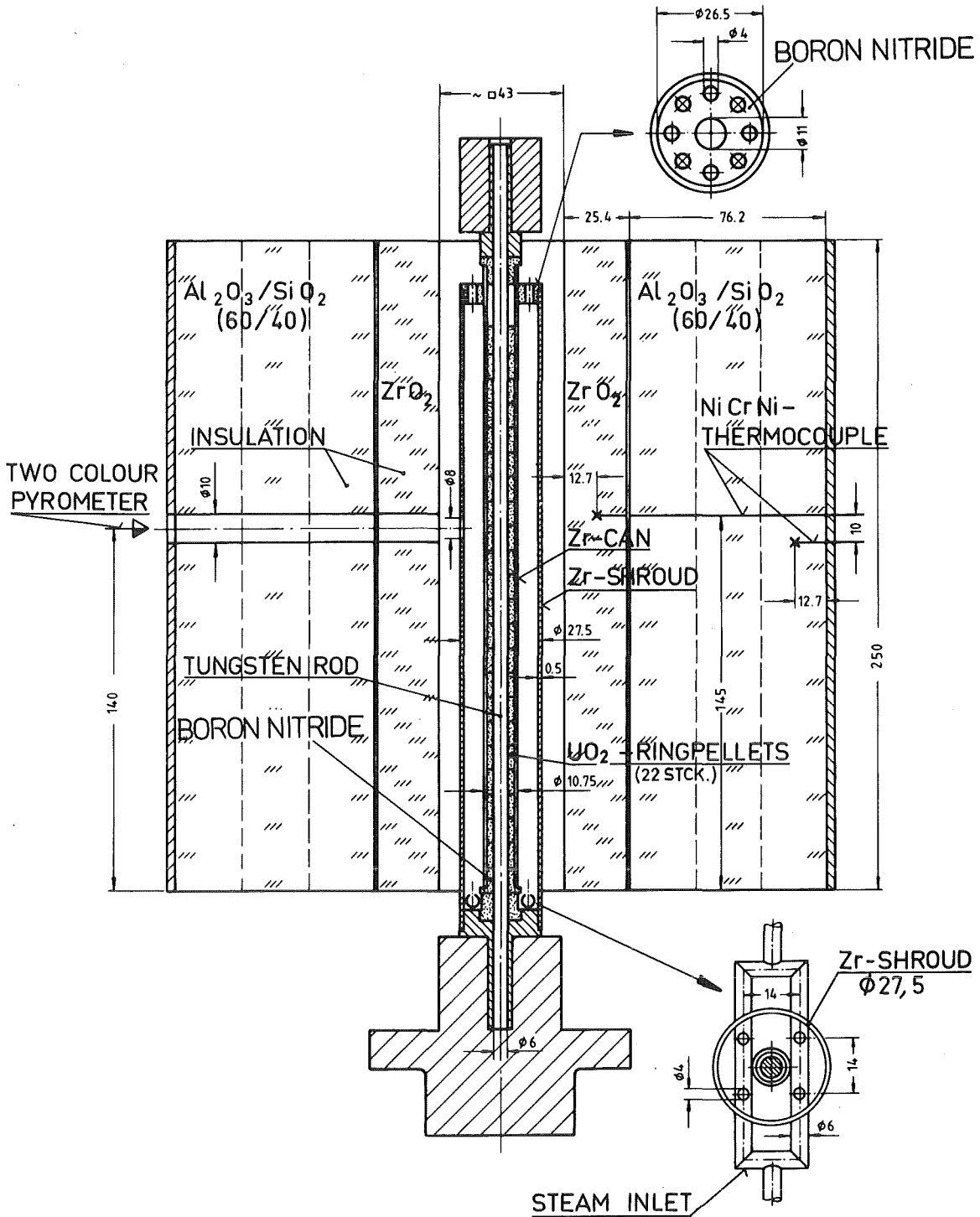


FIG. 1: SIDEVIEW OF THE EXPERIMENTAL ARRANGEMENT FOR TESTS ESSI-1.2.3



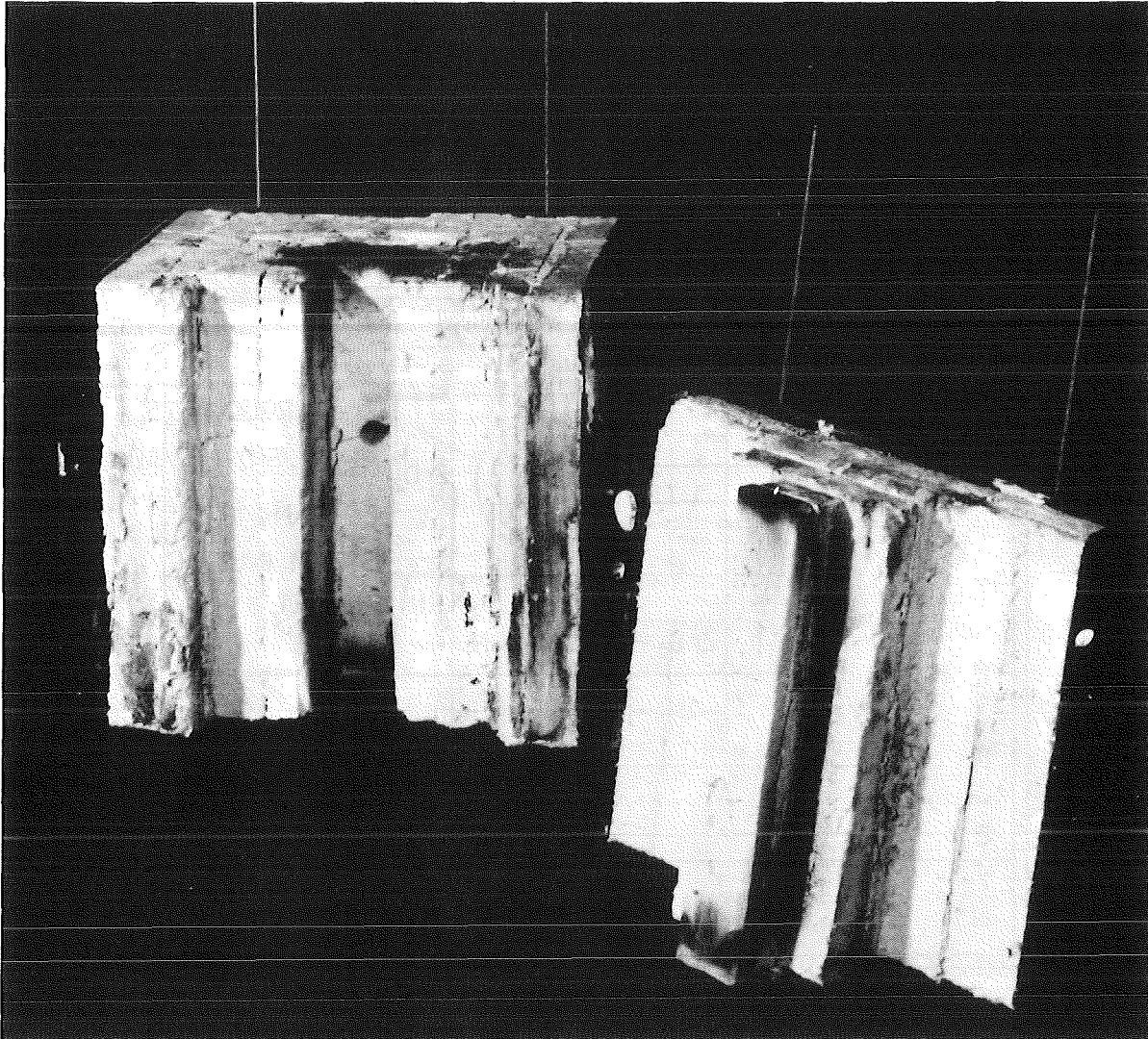
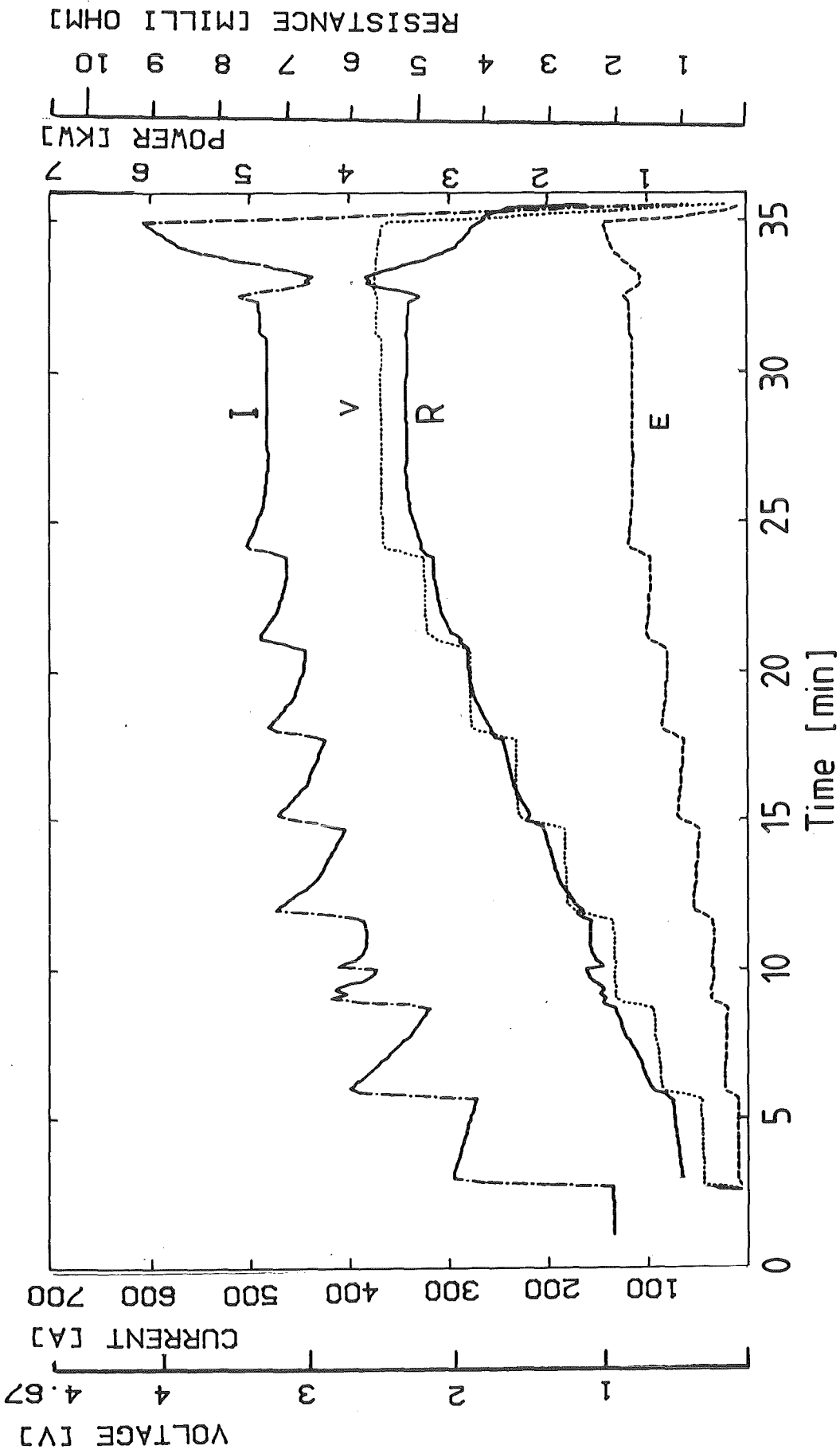


FIG. 3: FIBER CERAMIC INSULATION





HAGEN ET AL. KFK-REPORT 3507

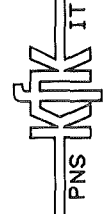
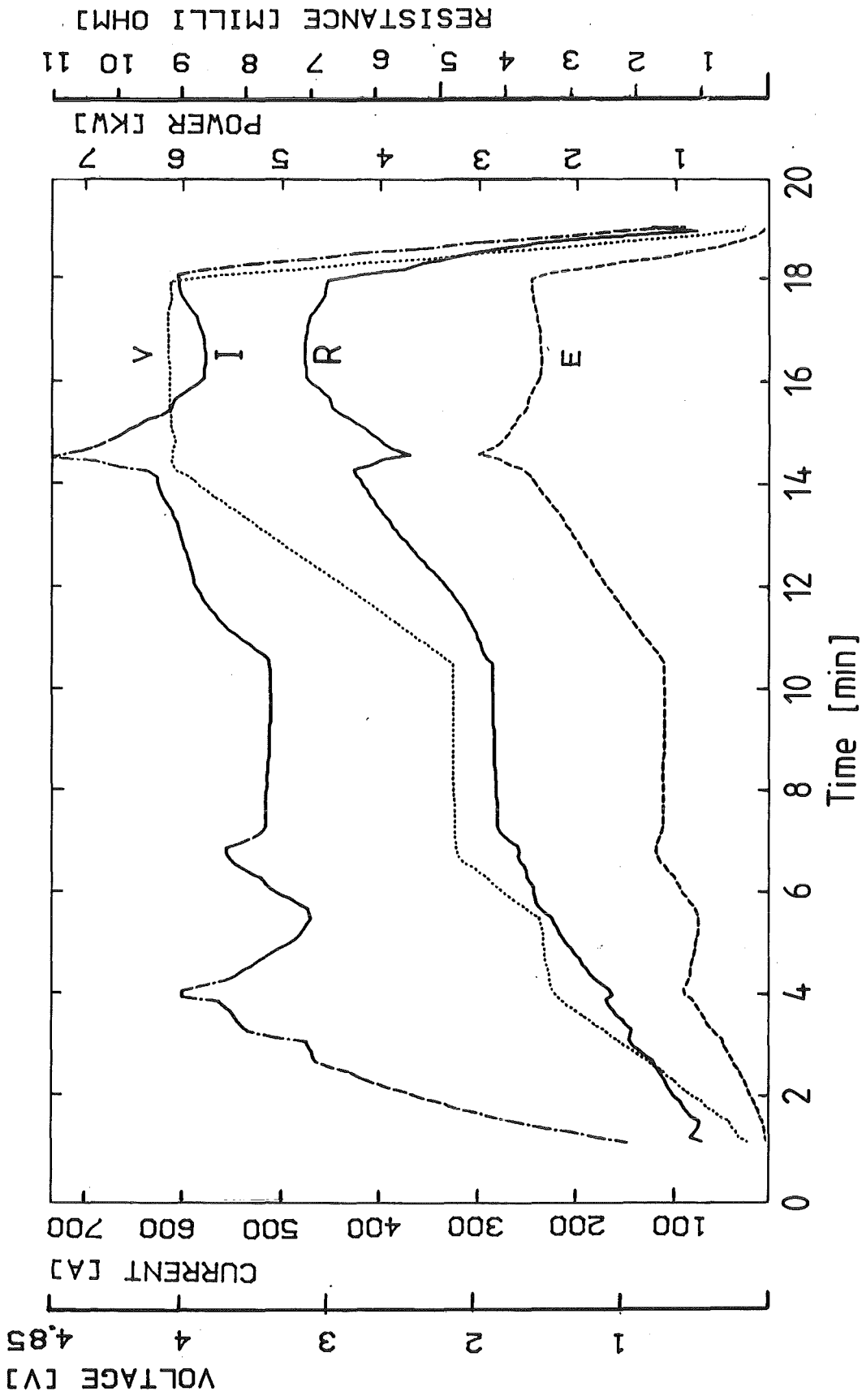
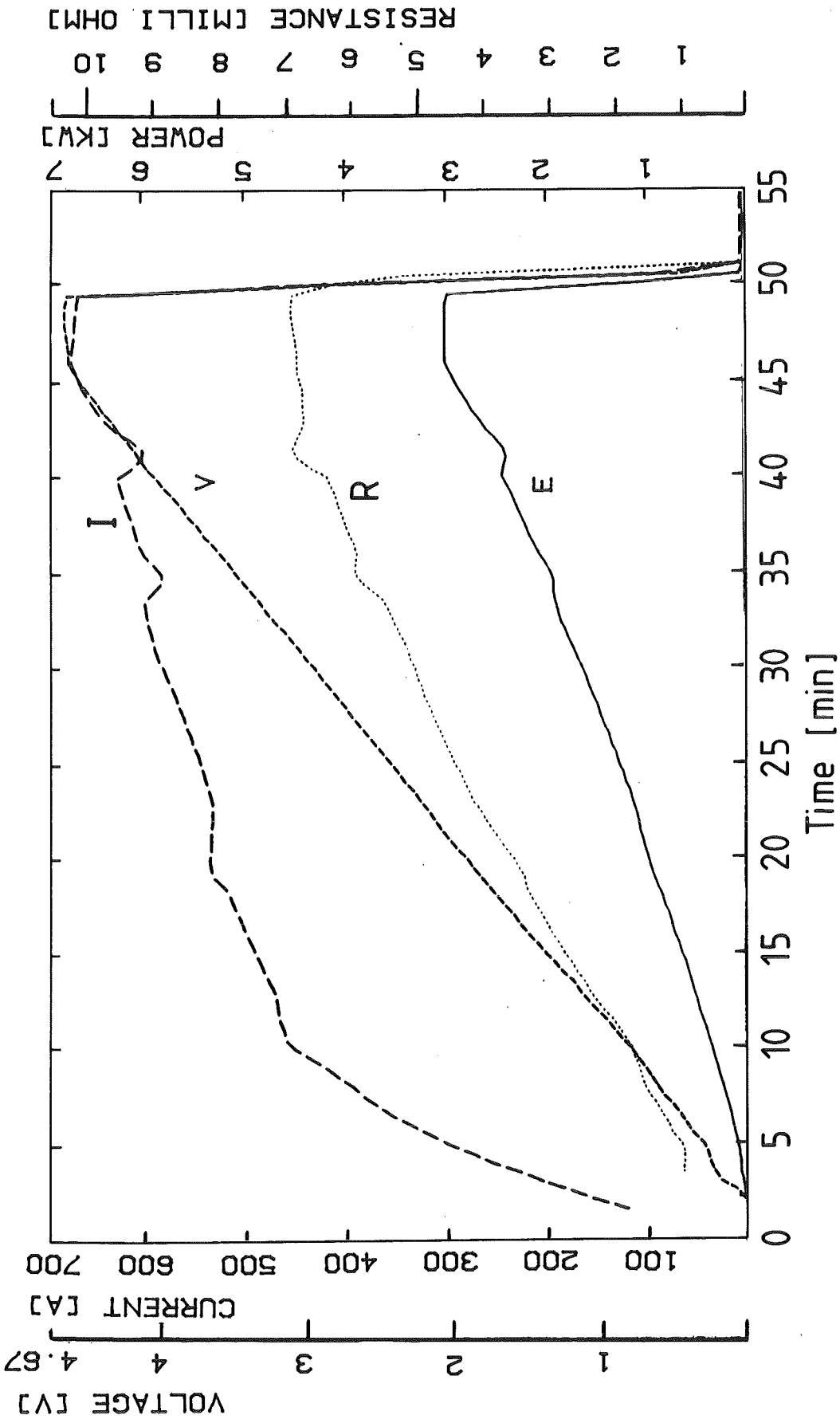


FIG. 4: VOLTAGE (V). CURRENT (I). RESISTANCE (R) AND ELECTRIC POWER (E) FOR TEST ESSI-1



HAGEN ET AL. KFK-REPORT 3507

FIG. 5: VOLTAGE (V), CURRENT (I), RESISTANCE (R) AND ELECTRIC POWER (E) FOR TEST ESS1-2



HAGEN ET AL. KFK-REPORT 3507



FIG. 6: VOLTAGE (V), CURRENT (I), RESISTANCE (R) AND ELECTRIC POWER (E) FOR TEST ESSI-3

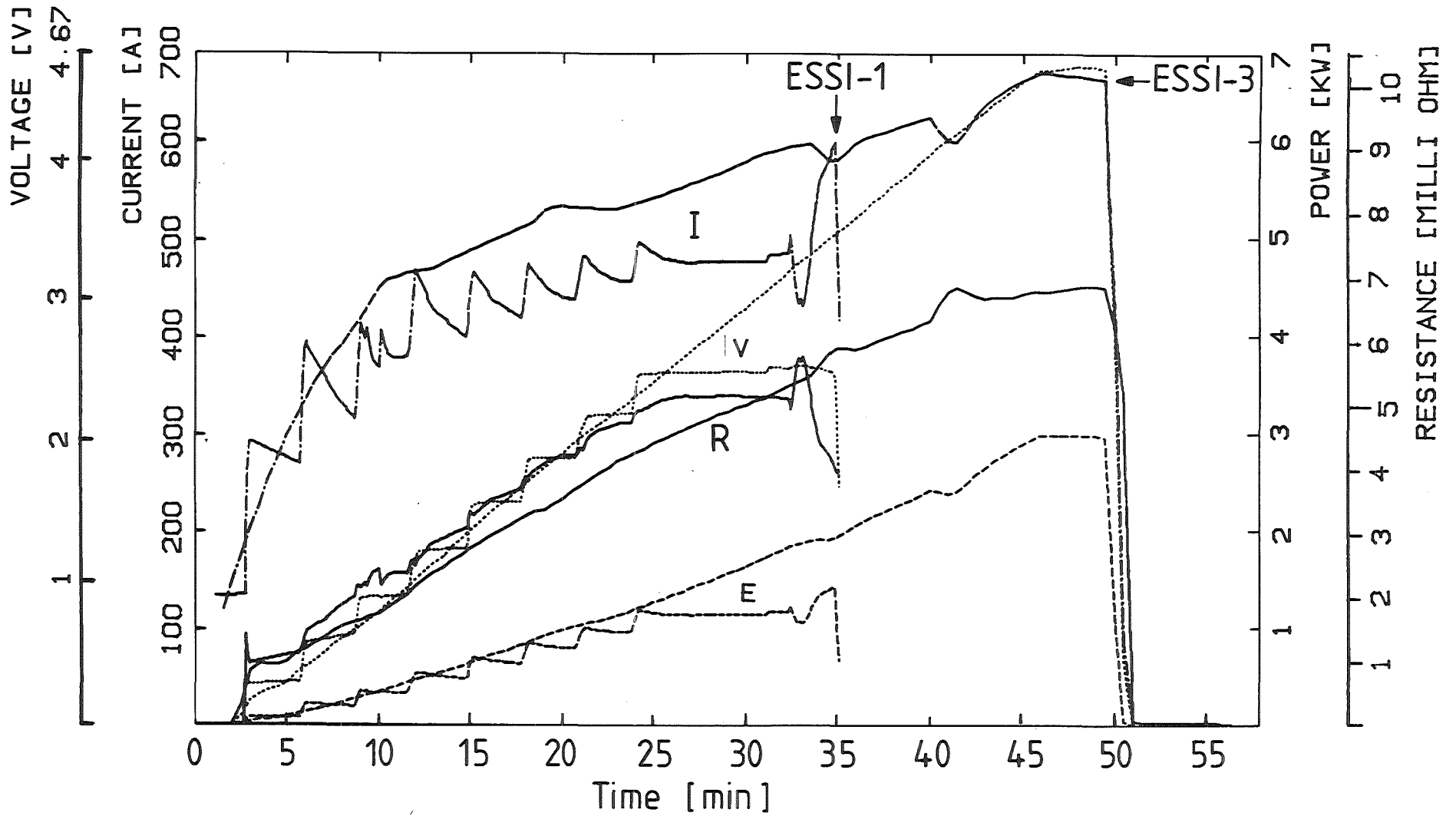


FIG. 7: COMPARISON OF THE VOLTAGES (V), CURRENTS (I), RESISTANCES (R) AND ELECTRIC POWERS (E) FOR ESSI-1 AND 3

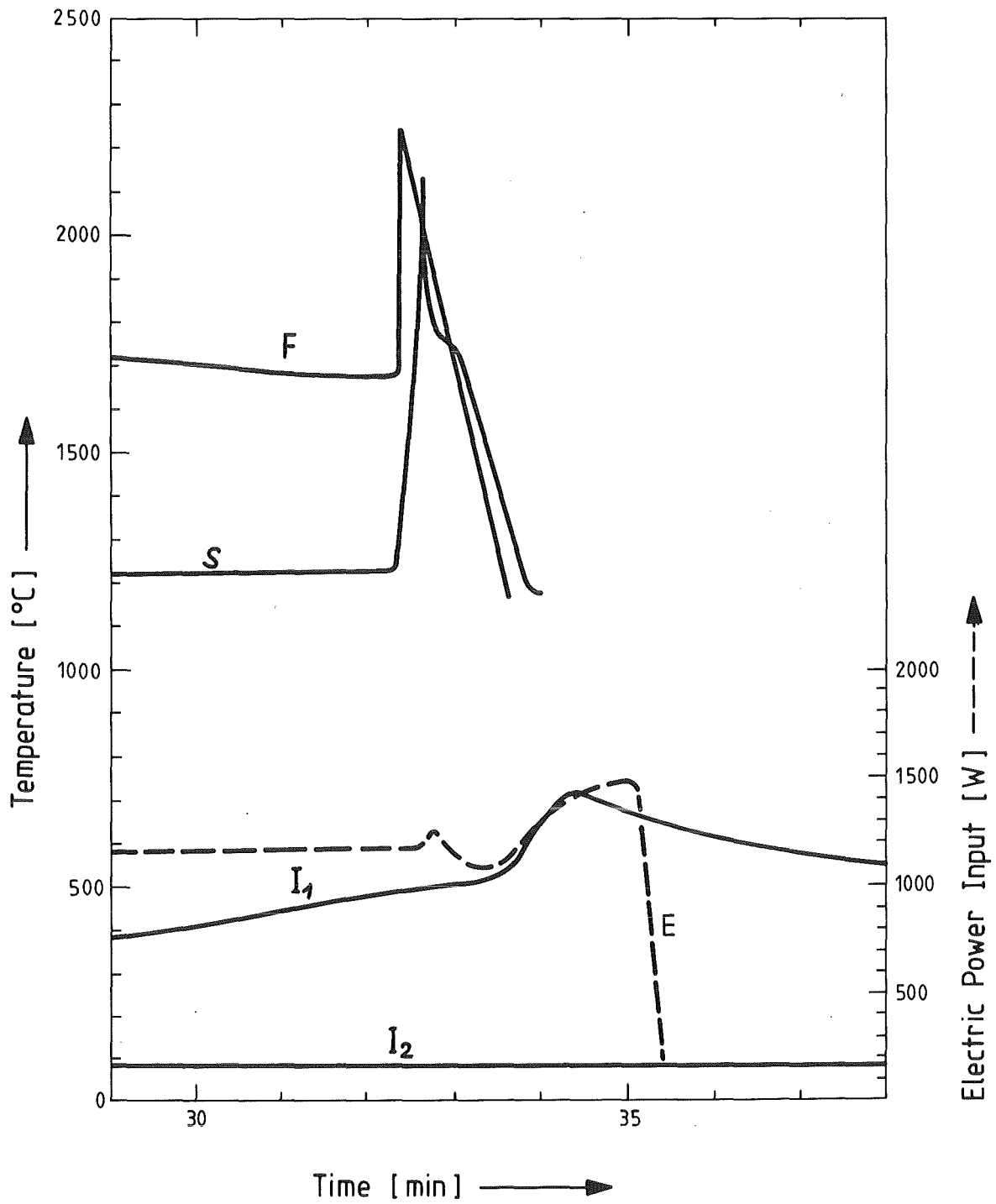


FIG. 8: TEMPERATURE OF THE FUEL ROD SIMULATOR (F), SHROUD (S), AND INSULATION (I1,I2) COMPARED TO THE ELECTRIC POWER INPUT (E) FOR ESSI-1

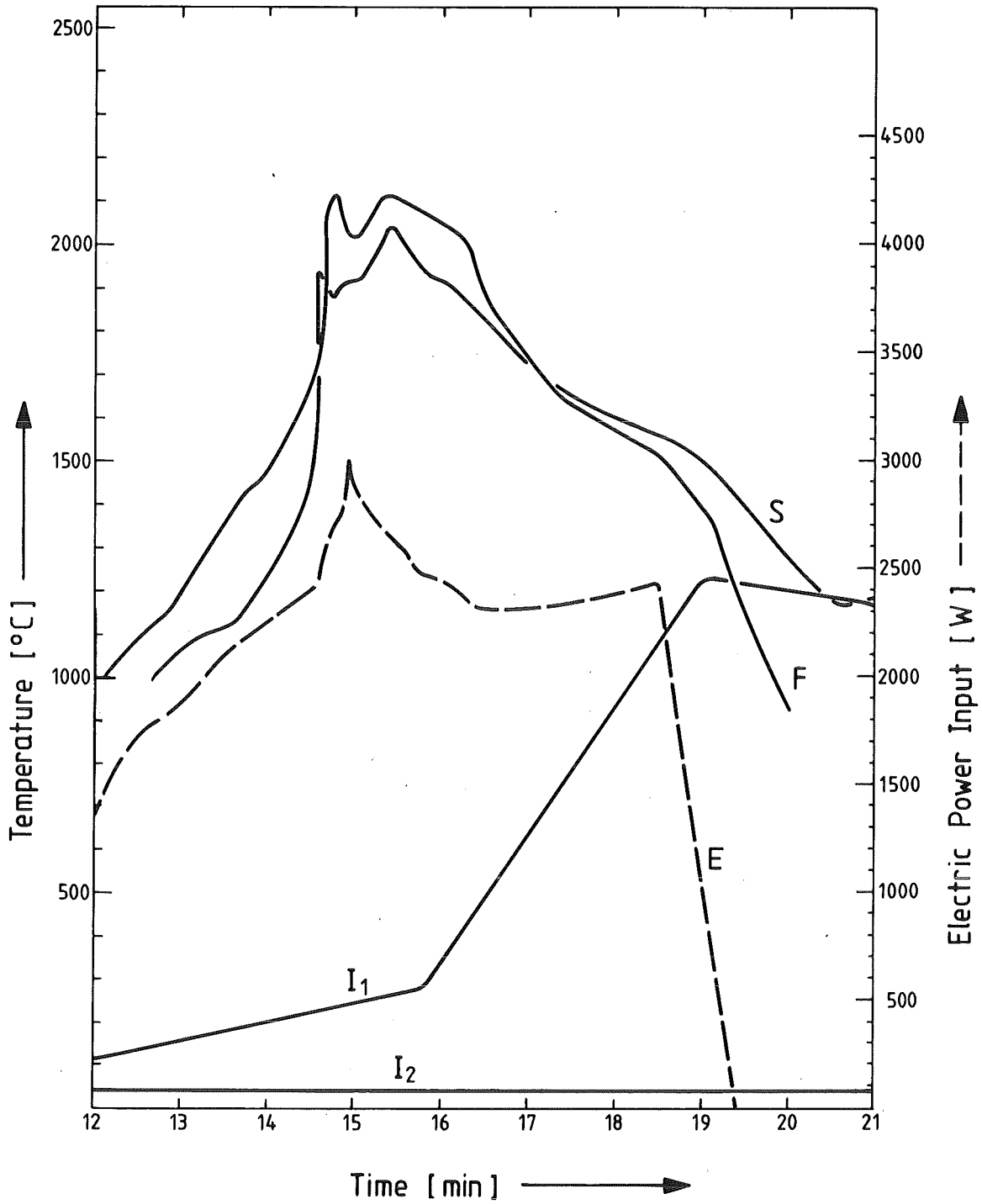


FIG. 9: TEMPERATURE OF THE FUEL ROD SIMULATOR (F), SHROUD (S), AND INSULATION (I1,I2) COMPARED TO THE ELECTRIC POWER INPUT (E) FOR ESSI-2

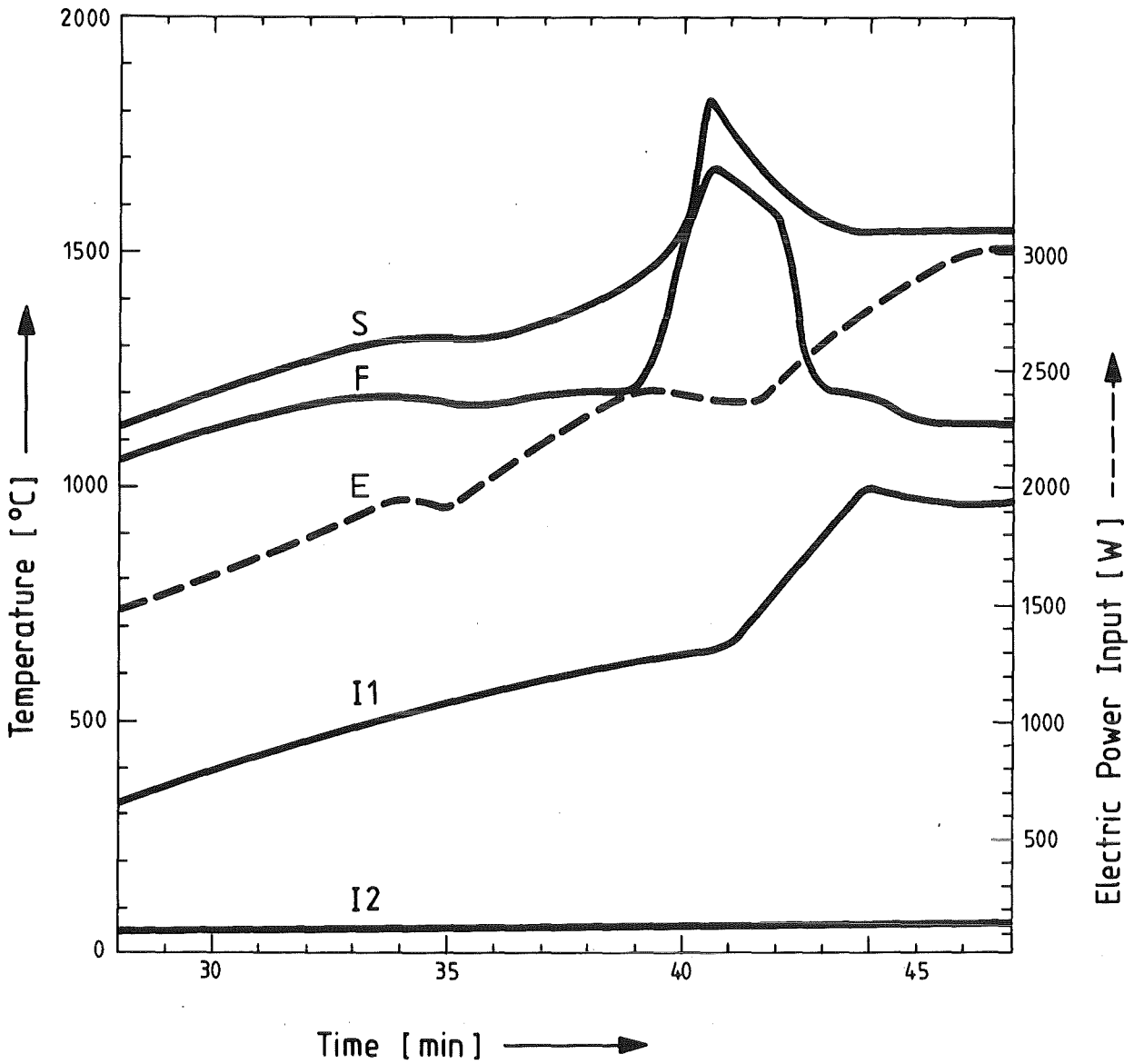


FIG.10: TEMPERATURE OF THE FUEL ROD SIMULATOR (F), SHROUD (S), AND INSULATION (I1,I2) COMPARED TO THE ELECTRIC POWER INPUT (E) FOR ESSI-3

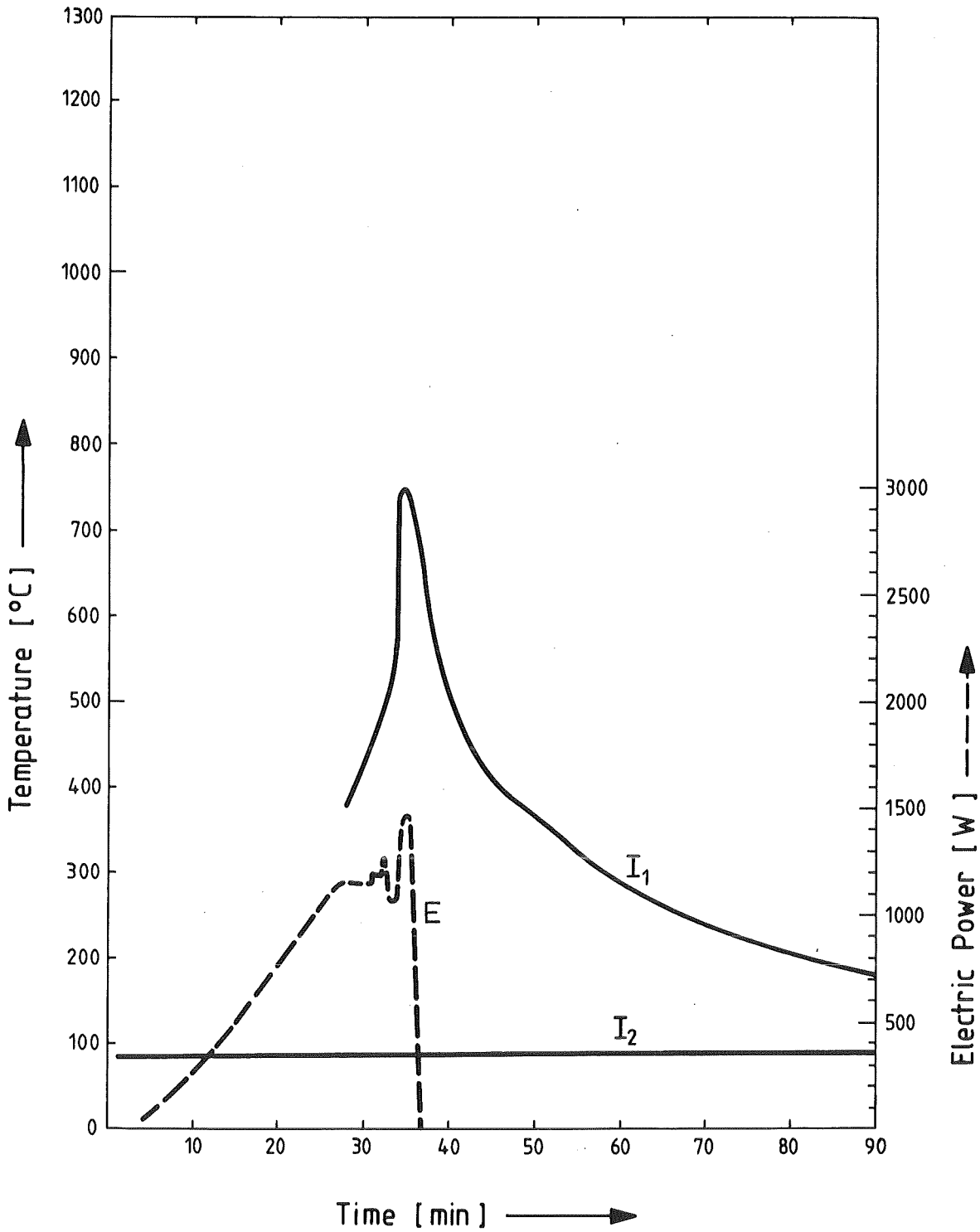


FIG.11: TEMPERATURES 1 CM FROM THE INNER SURFACE (I1) AND 1 CM FROM THE OUTER SURFACE (I2) OF THE INSULATION COMPARED TO ELECTRIC POWER (E) FOR ESSI-1



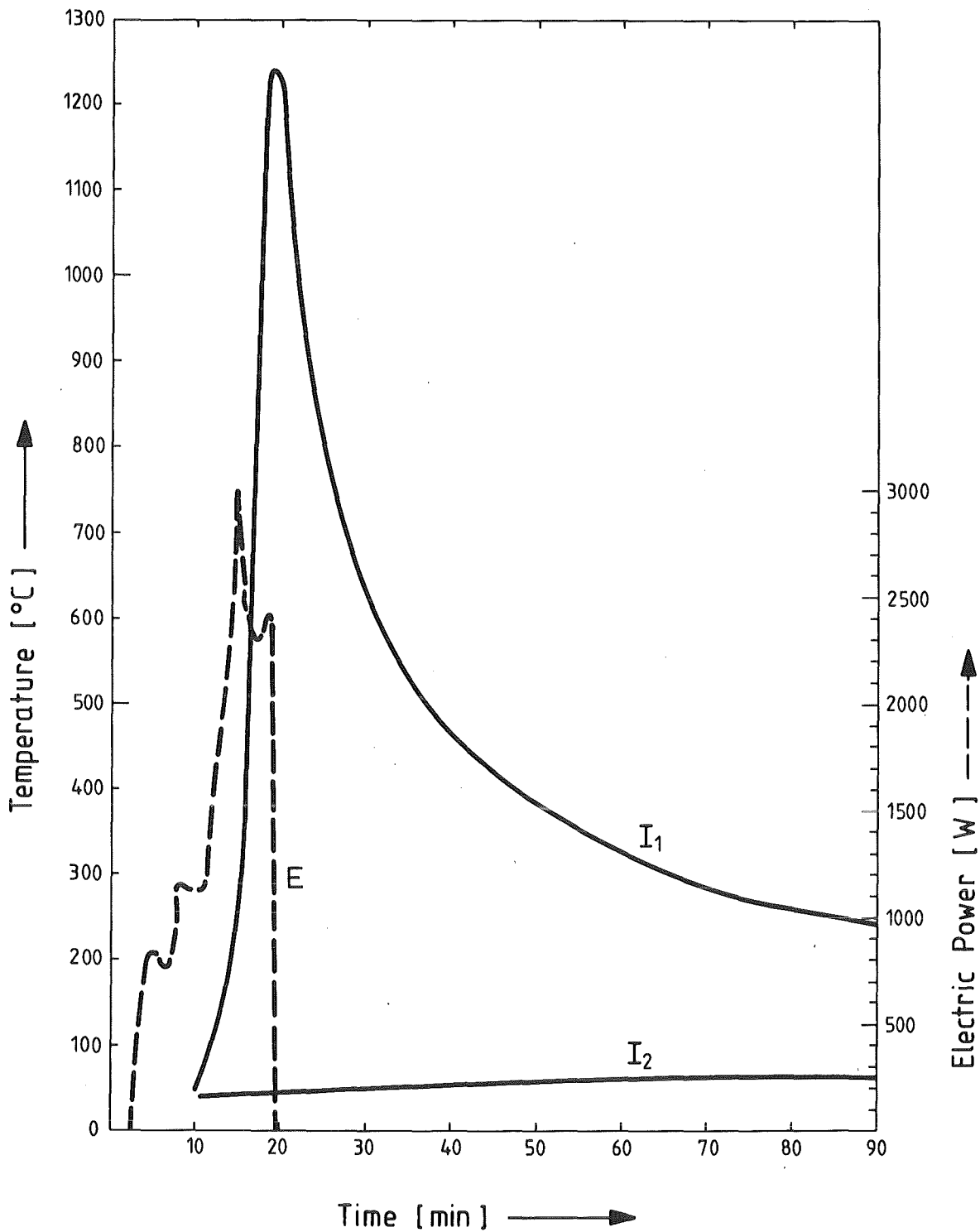


FIG. 12: TEMPERATURES 1 CM FROM THE INNER SURFACE (I1) AND 1 CM FROM THE OUTER SURFACE (I2) OF THE INSULATION COMPARED TO ELECTRIC POWER (E) FOR ESSI-2

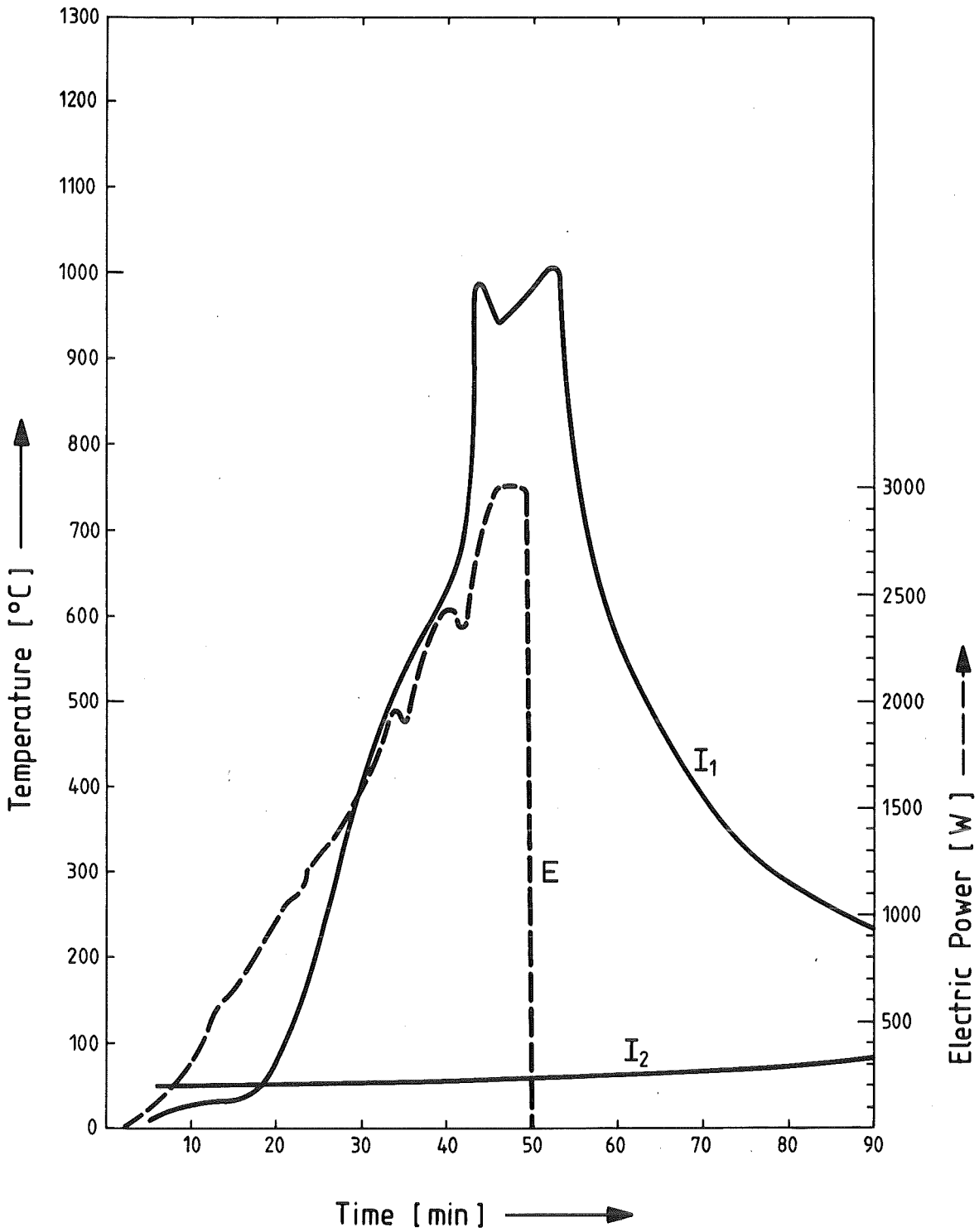


FIG. 13: TEMPERATURES 1 CM FROM THE INNER SURFACE (I1) AND 1 CM FROM THE OUTER SURFACE (I2) OF THE INSULATION COMPARED TO ELECTRIC POWER (E) FOR ESSI-3

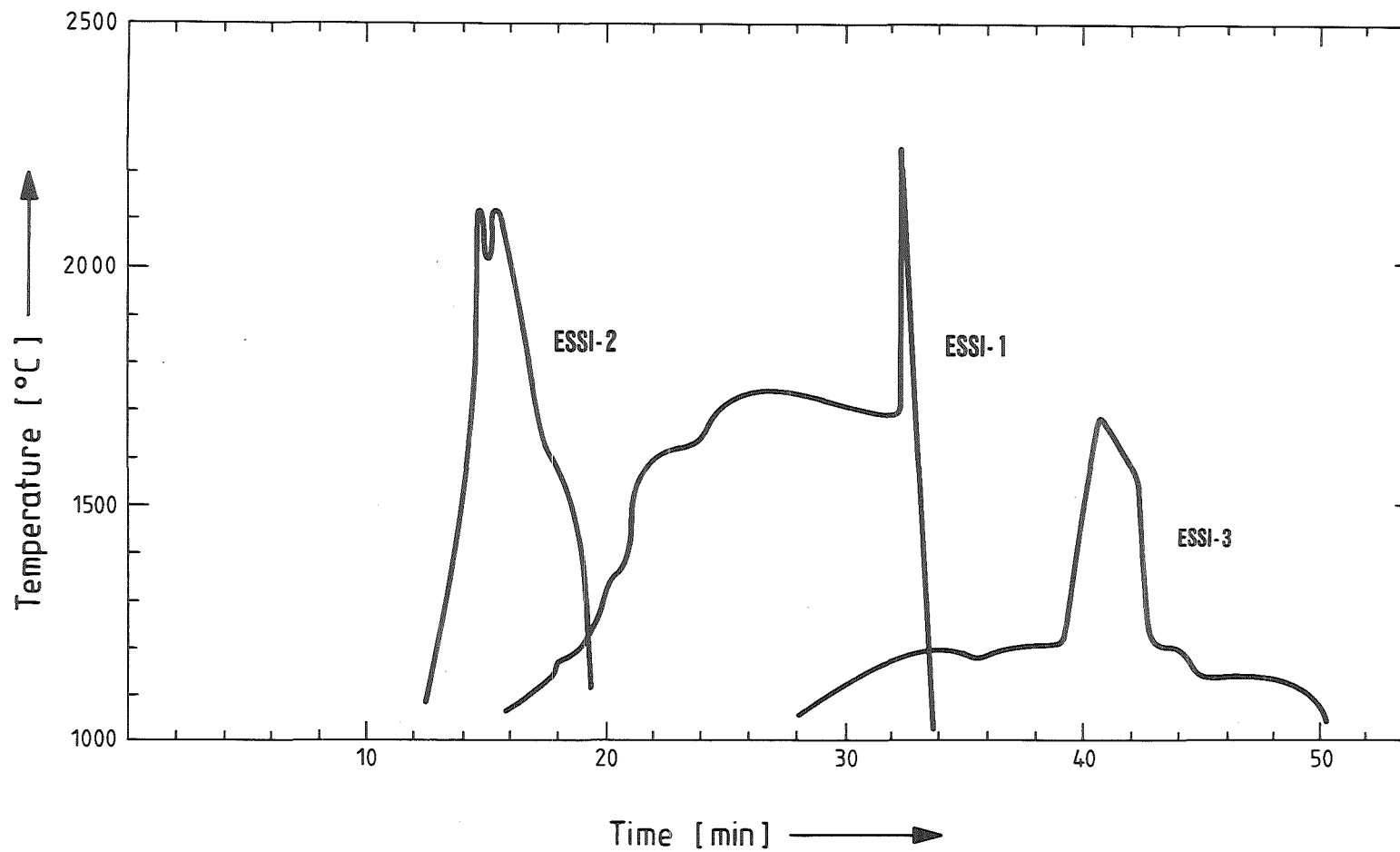


FIG.14: COMPARISON OF FUEL ROD SIMULATOR TEMPERATURES FOR ESSI-1.2.3.

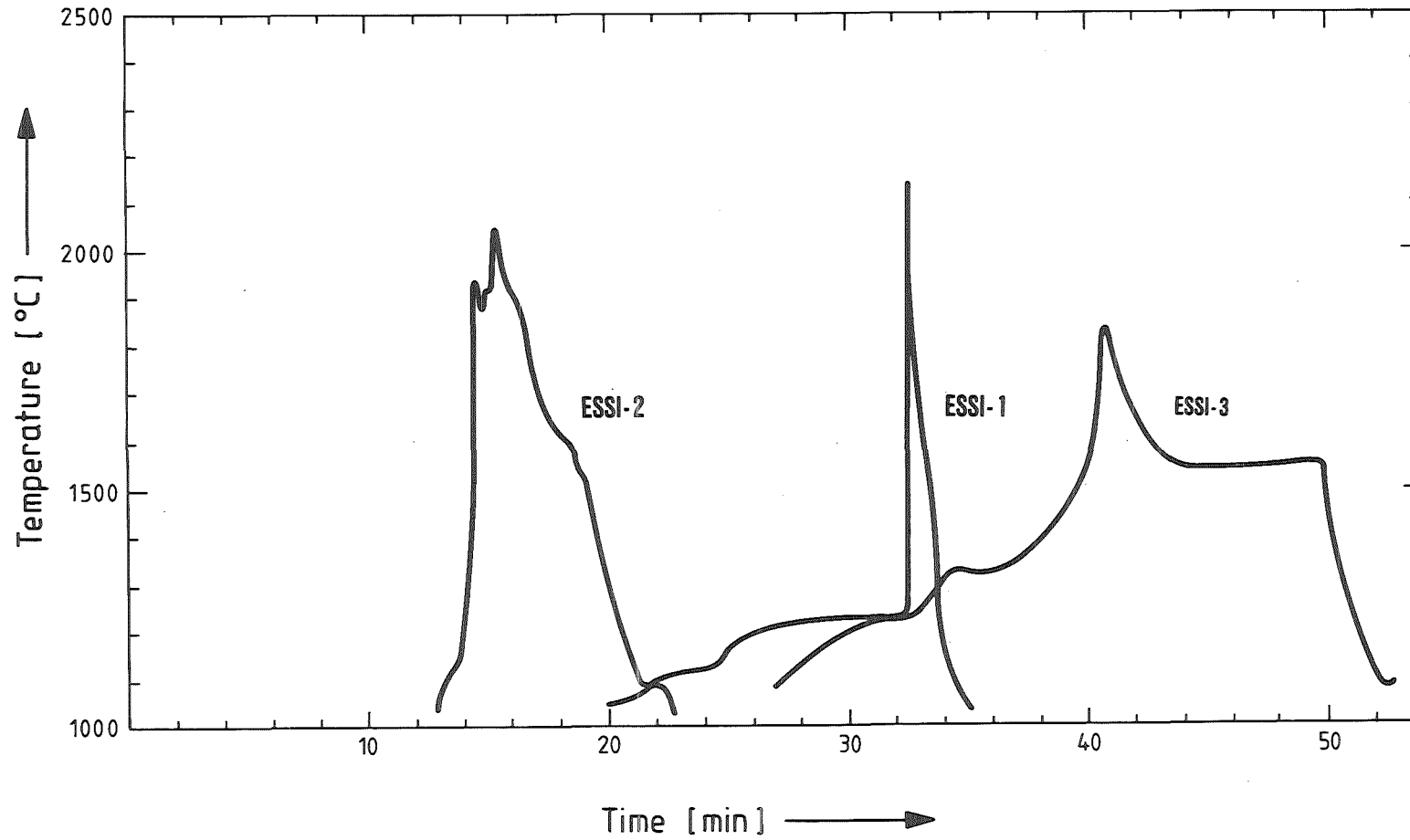


FIG. 15: COMPARISON OF SHROUD TEMPERATURES FOR ESSI-1.2.3.

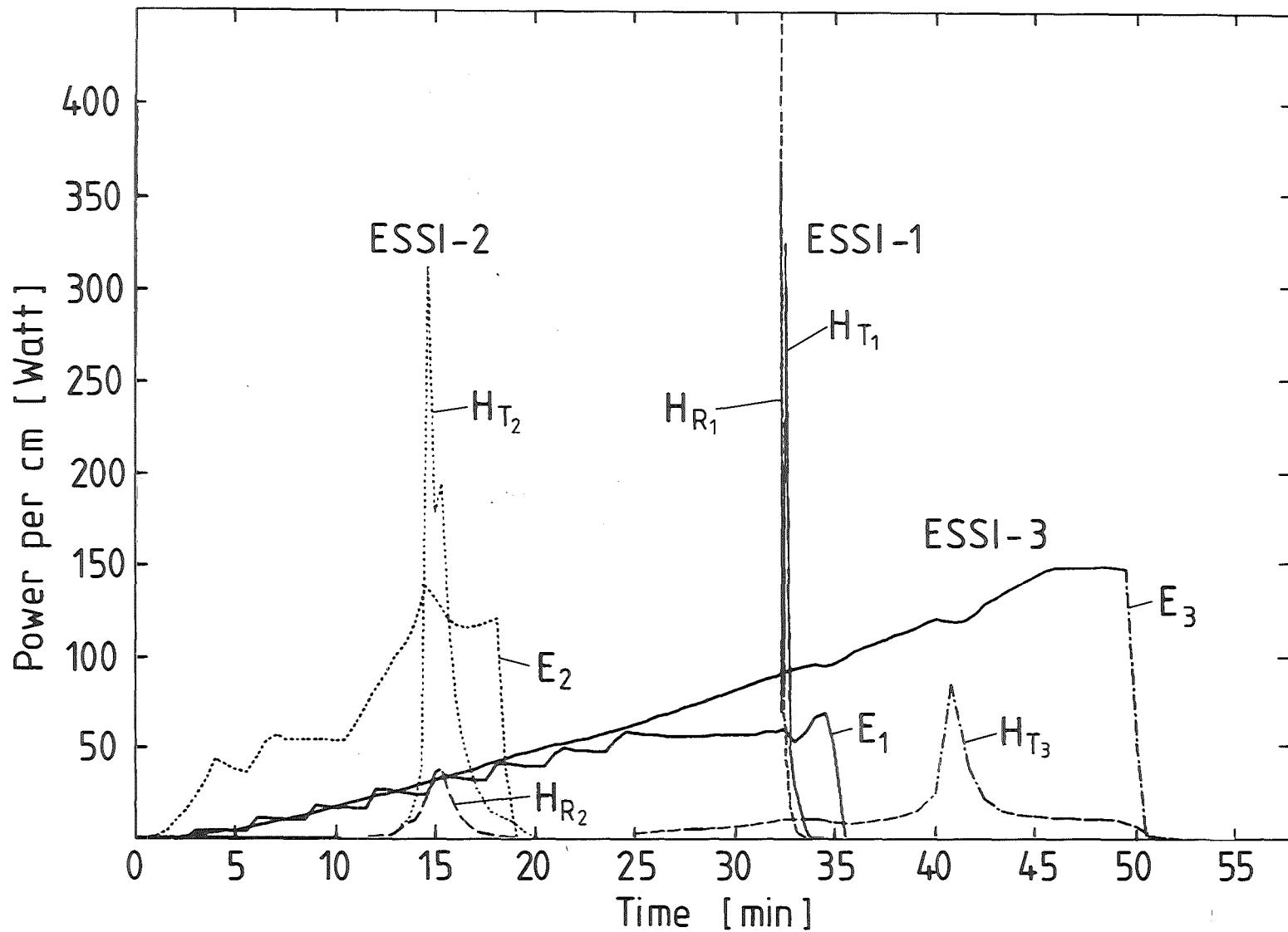


FIG. 16: COMPARISON OF THE MULTRAN CALCULATED REACTION POWERS FOR THE RODS (HR) AND SHROUDS (HT) WITH THE ELECTRIC INPUT POWERS OF ESSI-1,2,3.

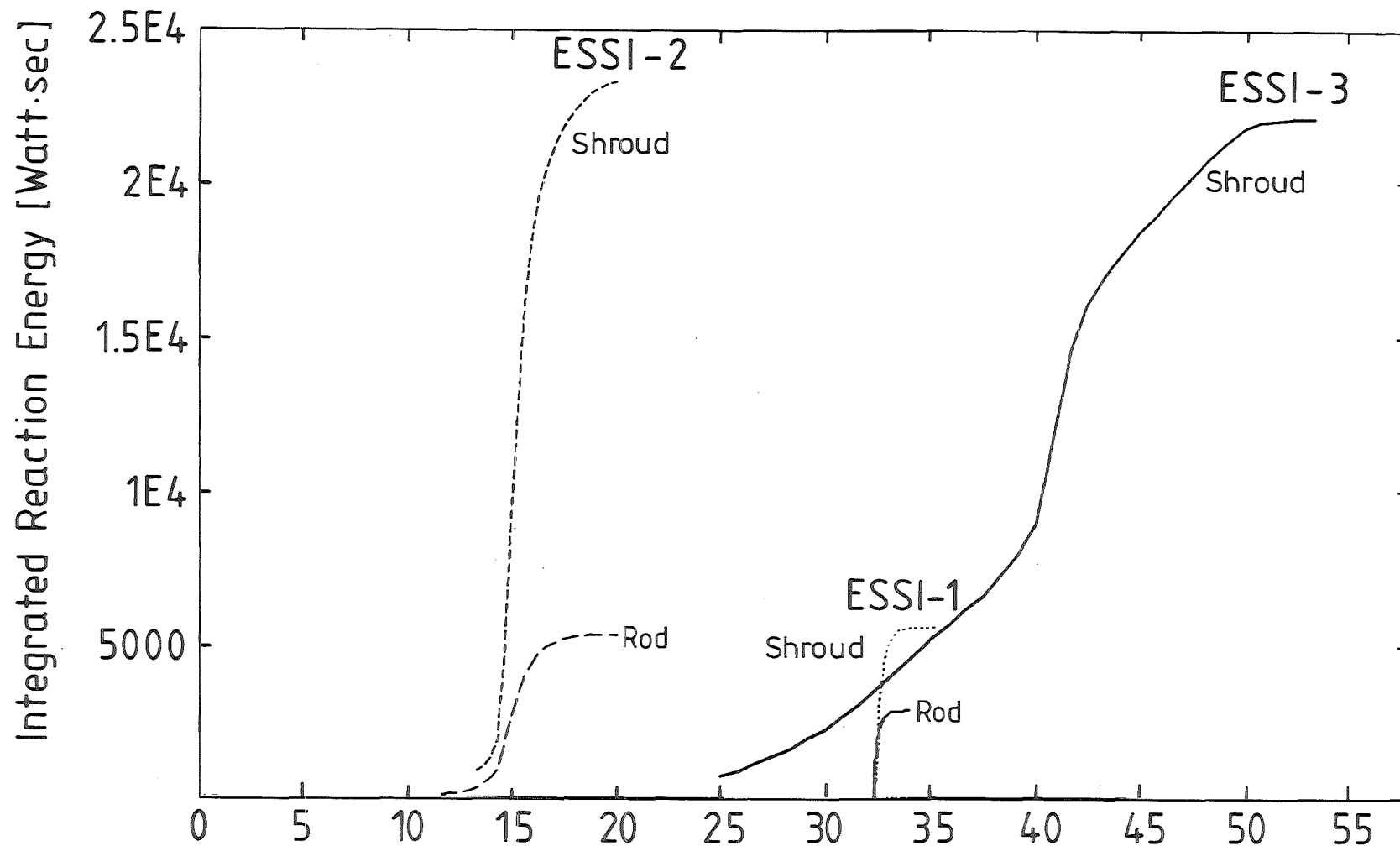


FIG.17: COMPARISON OF THE MULTRAN CALCULATED TOTAL OXIDATION GENERATED ENERGY AS A FUNCTION OF TIME FOR ESSI-1,2,3.

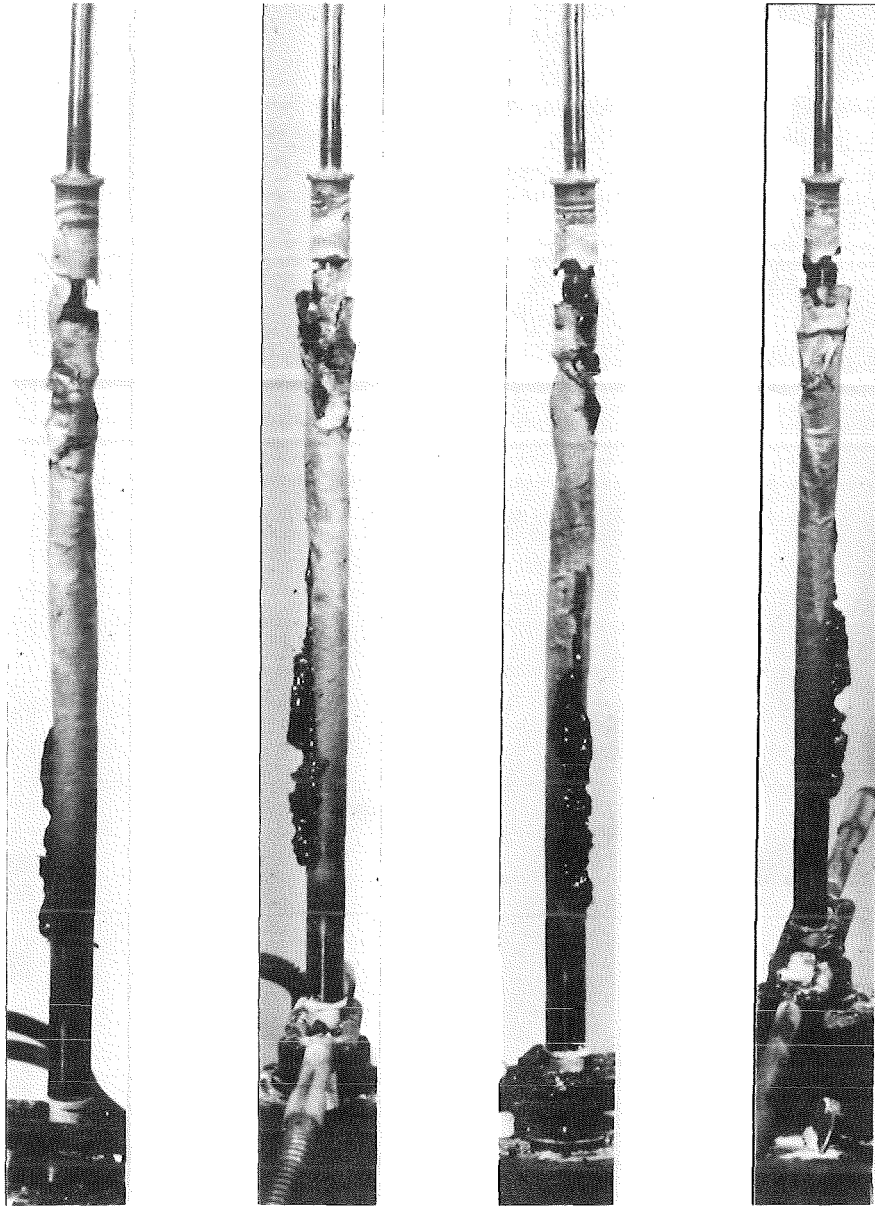


FIG.18: POSTTEST APPEARANCE OF THE ESS1-1 FUEL ROD SIMULATOR SHOWN FROM FOUR ORIENTATIONS.

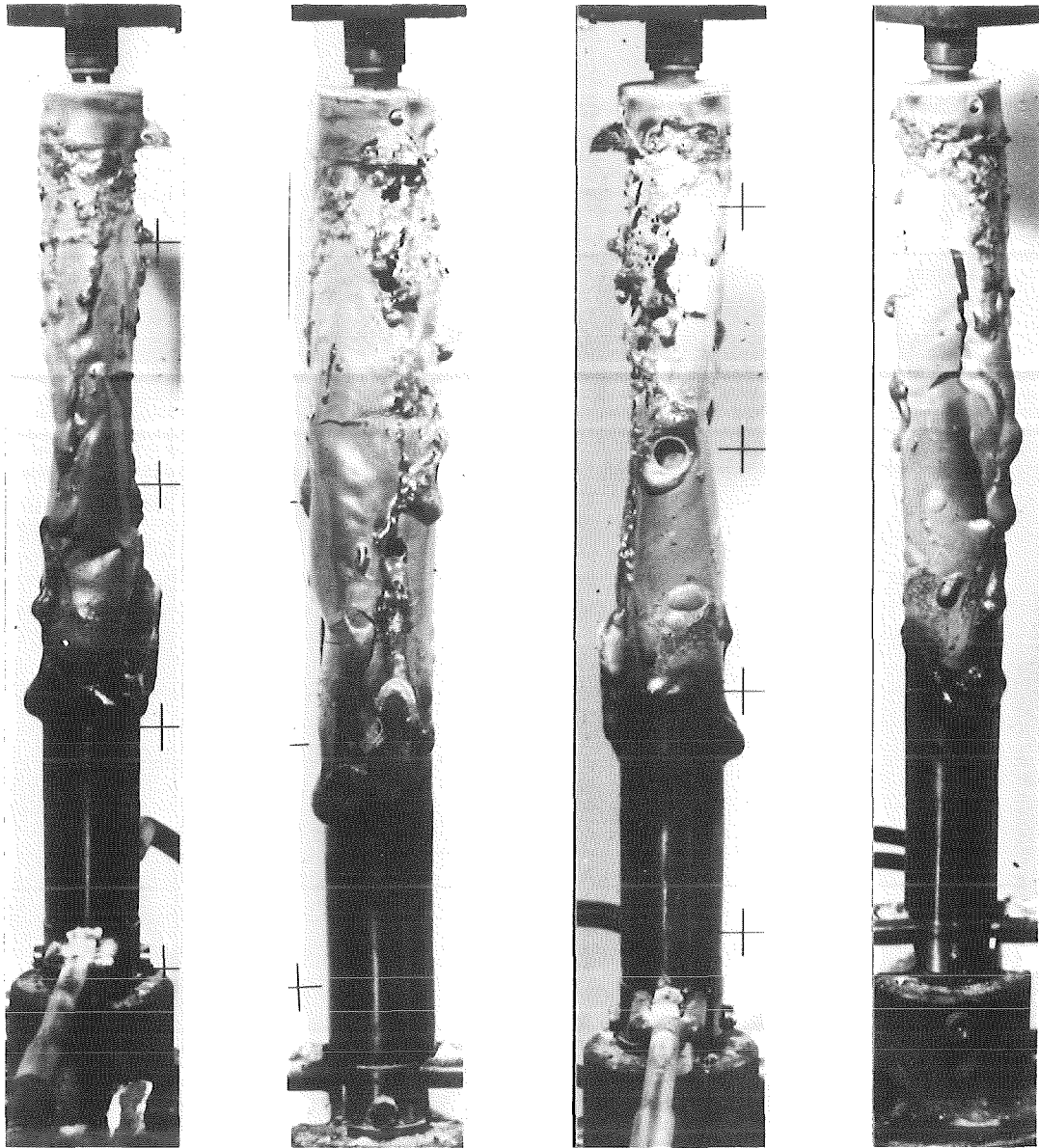


FIG. 19: POSTTEST APPEARANCE OF THE ESS1-1 SHROUD  
SHOWN FROM FOUR ORIENTATIONS.



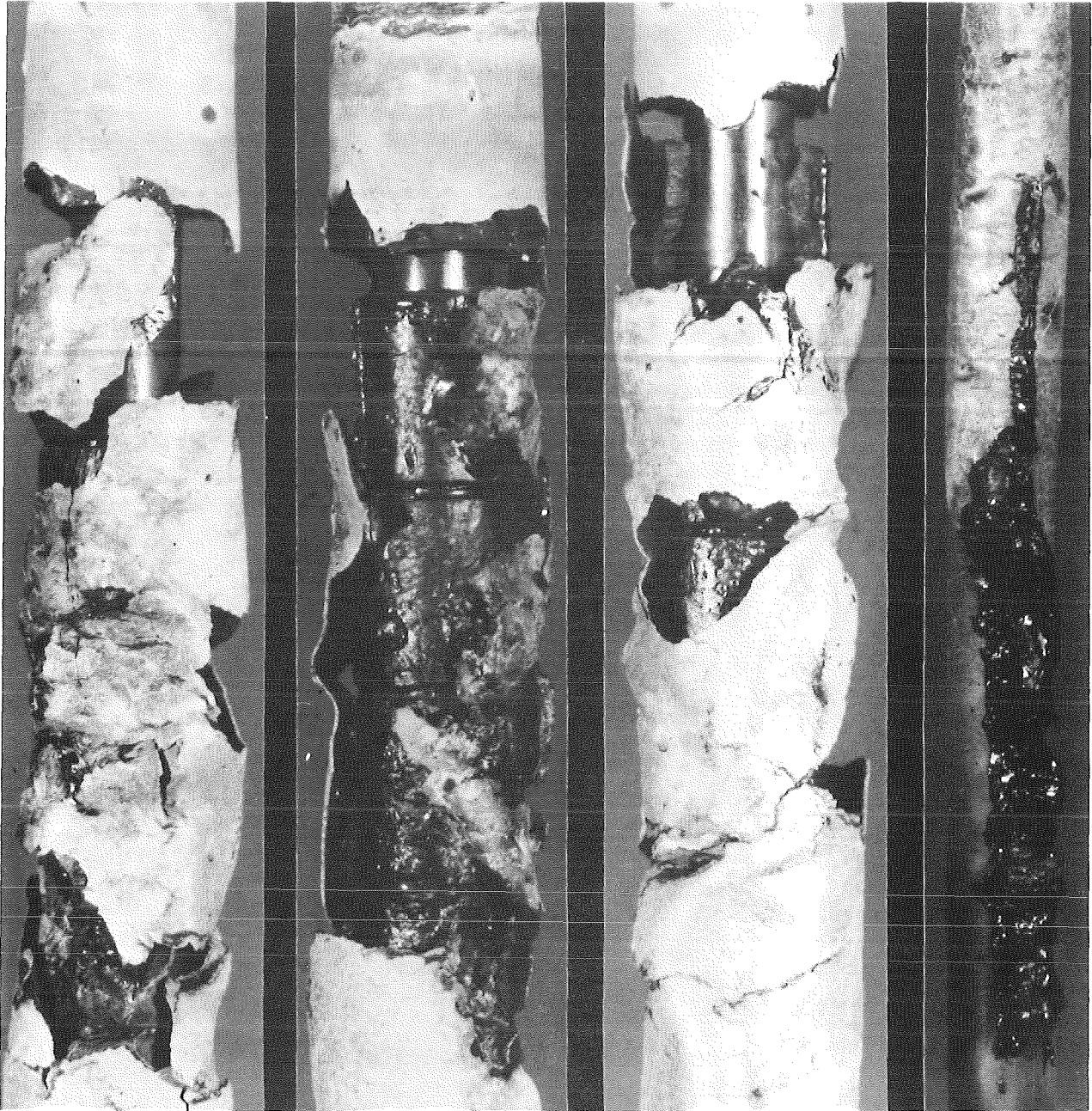


FIG. 20: DETAILS OF THE FUEL ROD SIMULATOR POSTTEST APPEARANCE FOR ESSI-1

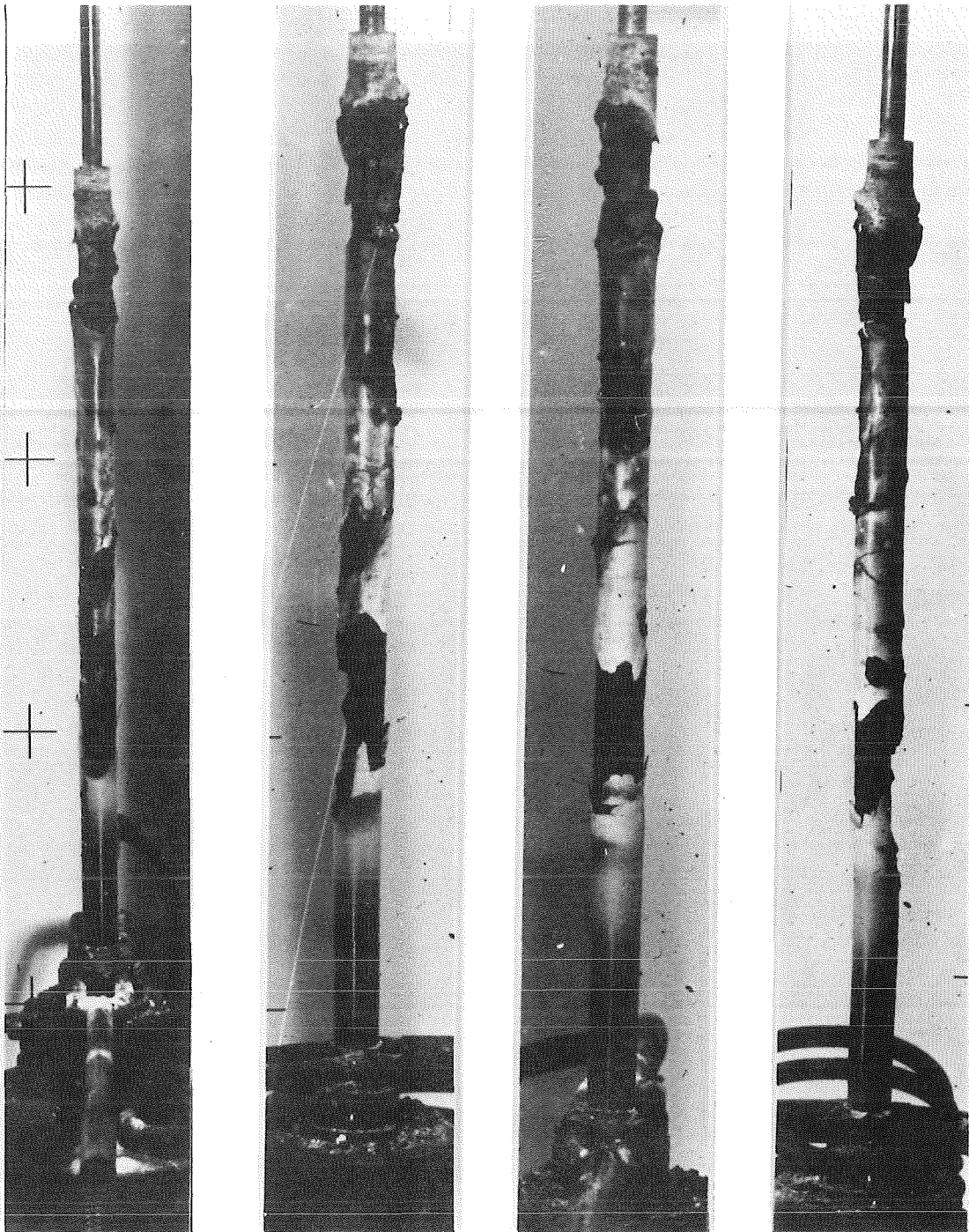


FIG. 21: POSTTEST APPEARANCE OF THE ESS1-2 FUEL ROD SIMULATOR SHOWN FROM FOUR ORIENTATIONS.



FIG. 22: POSTTEST APPEARANCE OF THE ESSI-2 SHROUD  
SHOWN FROM FOUR ORIENTATIONS.

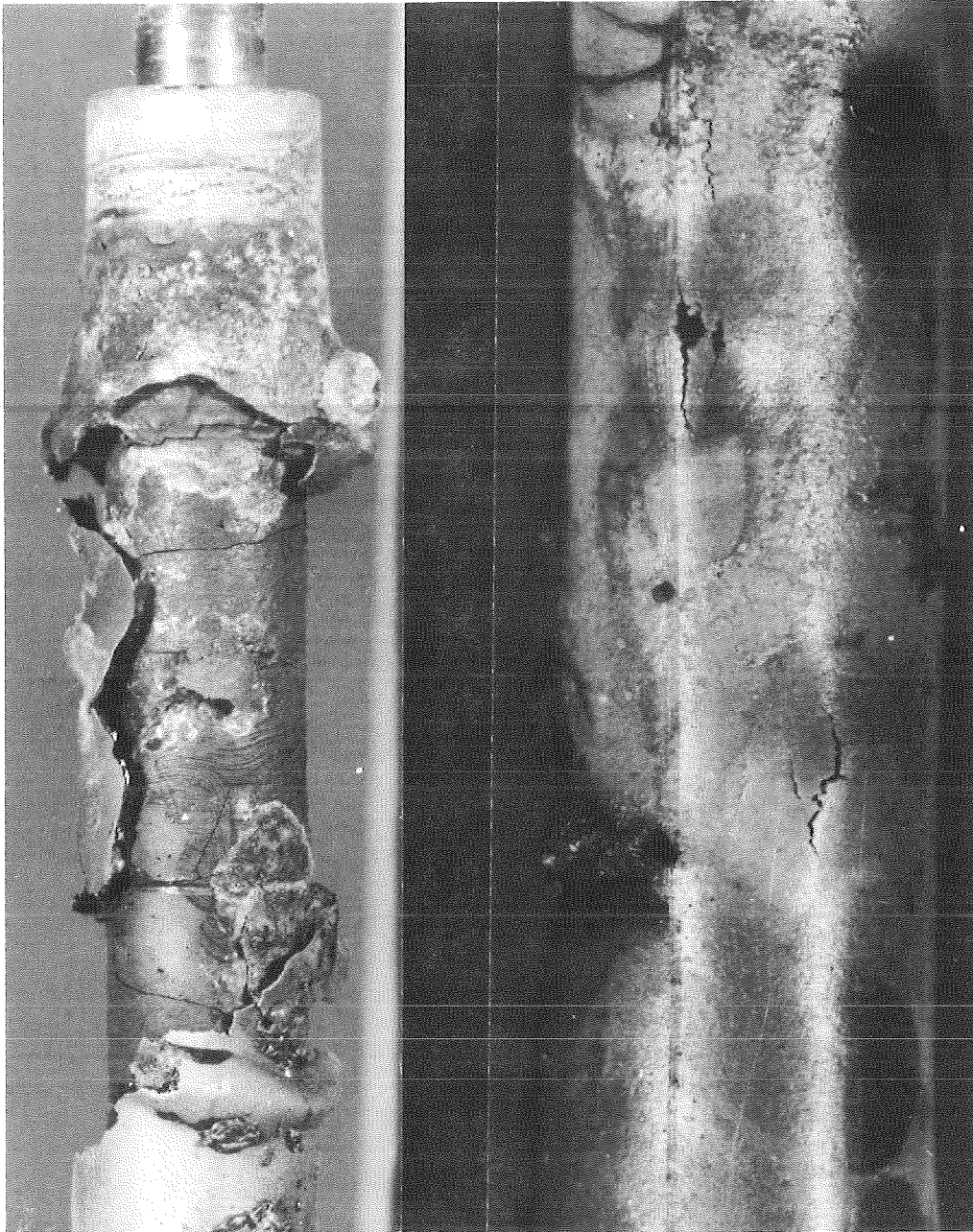


FIG.23: DETAILS OF THE FUEL ROD SIMULATOR POSTTEST APPEARANCE FOR ESSI-2

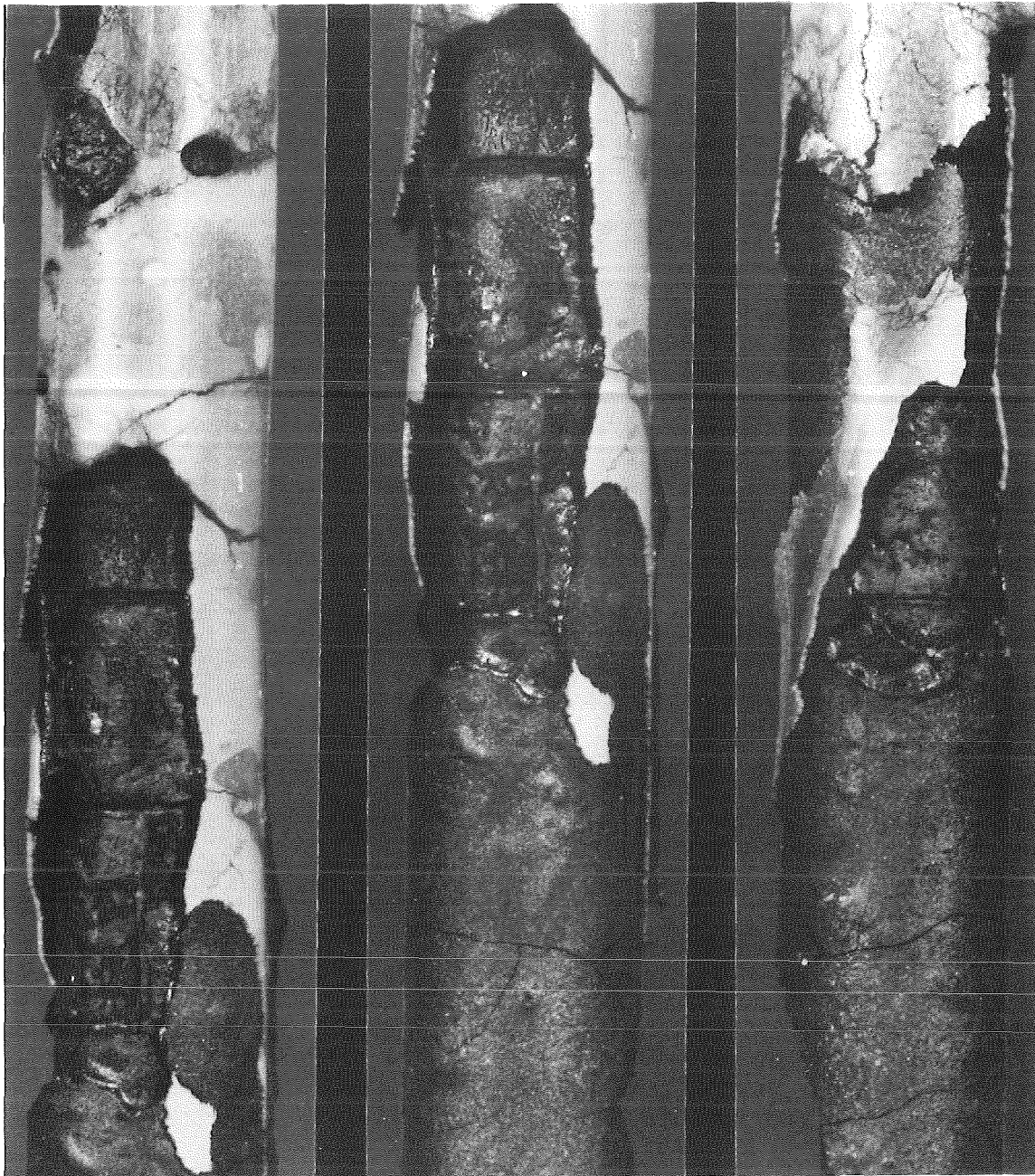


FIG.24: DETAILS OF THE FUEL ROD SIMULATOR POSTTEST APPEARANCE FOR ESSI-2

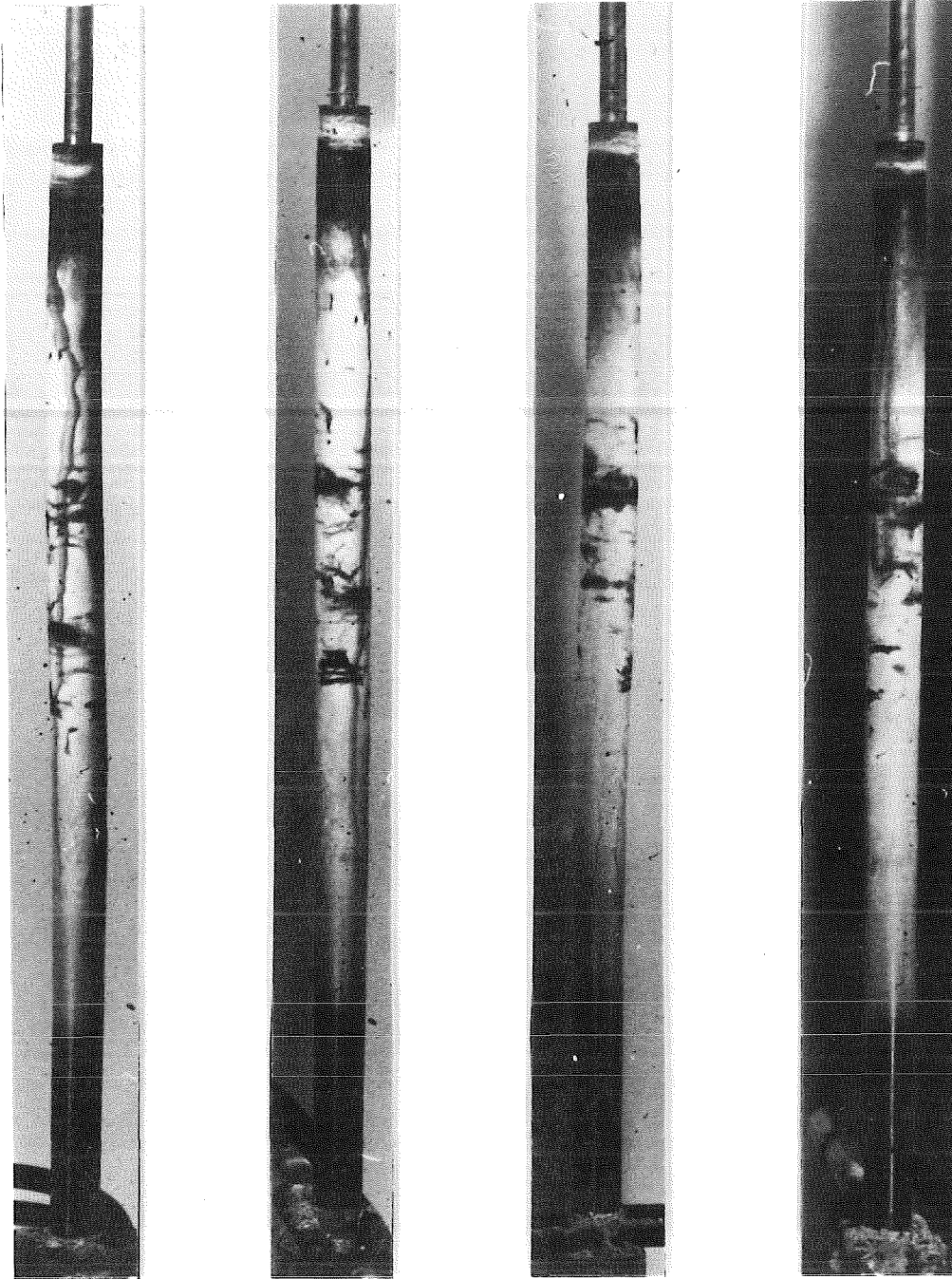


FIG.25: POSTTEST APPEARANCE OF THE ESS1-3 FUEL ROD SIMULATOR SHOWN FROM FOUR ORIENTATIONS.

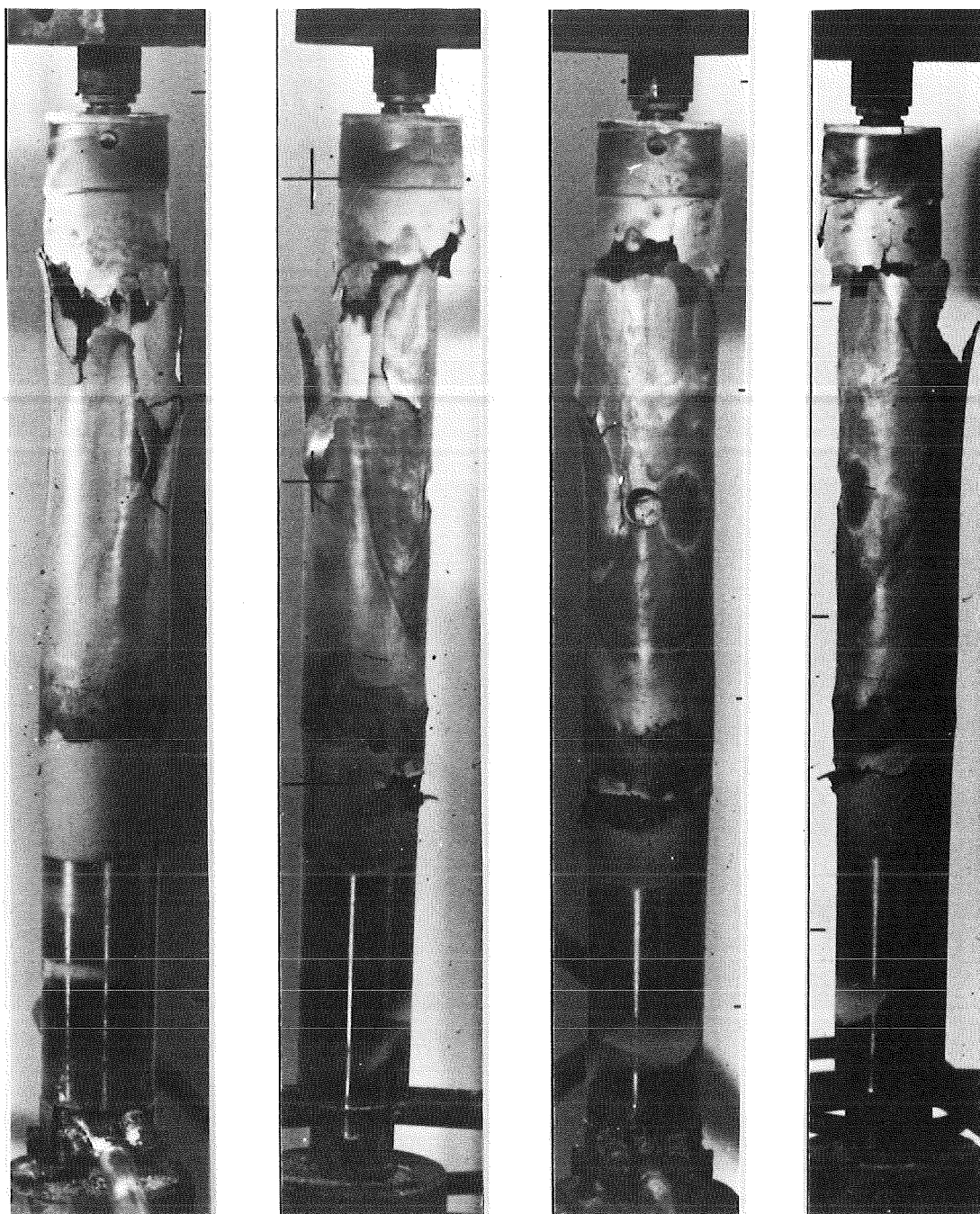


FIG. 26: POSTTEST APPEARANCE OF THE ESSI-3 SHROUD SHOWN FROM FOUR ORIENTATIONS.

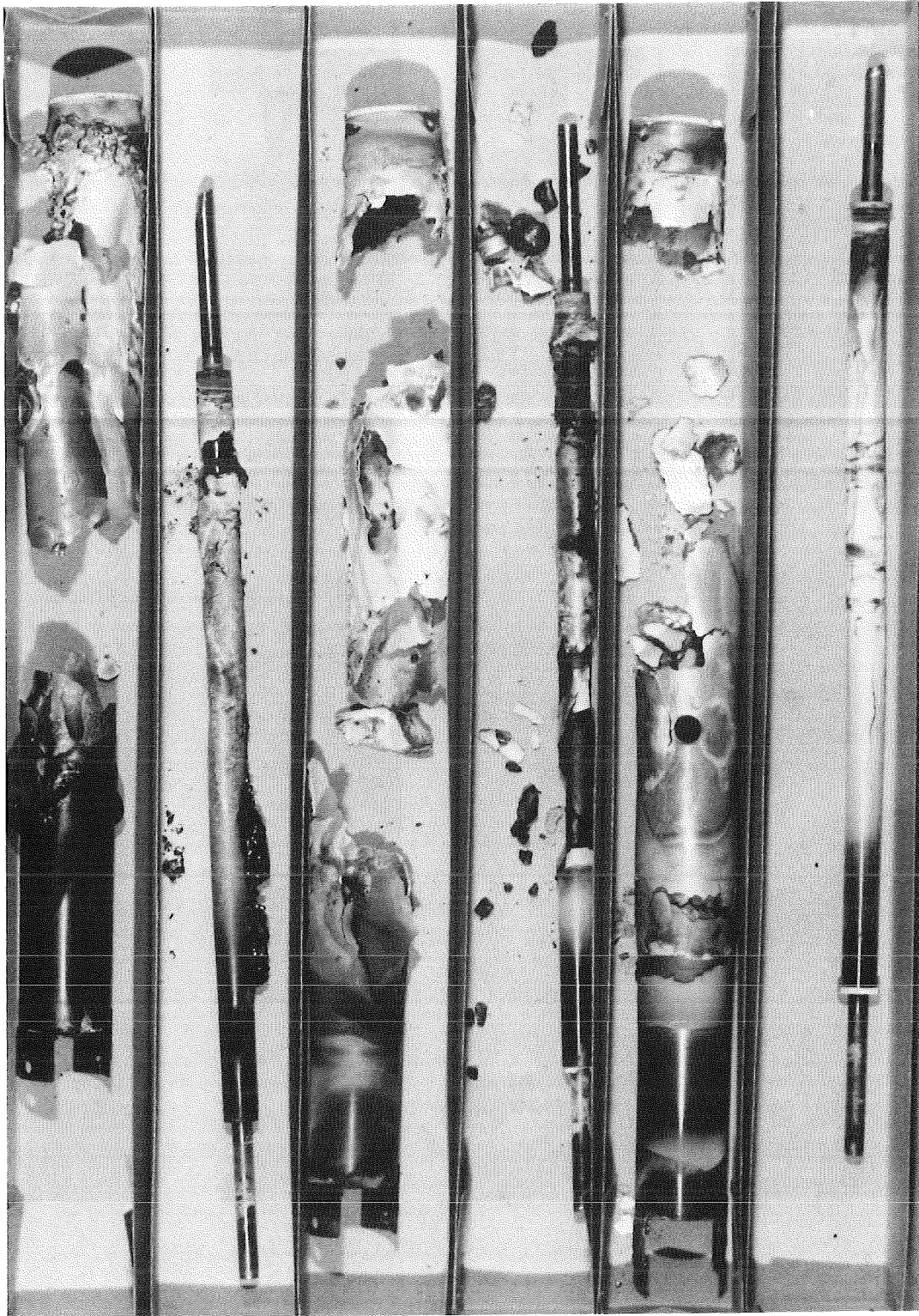


FIG.27: FUEL ROD SIMULATORS AND SHROUDS FROM TESTS ESSI-1.2.3  
AFTER DISMANTLING



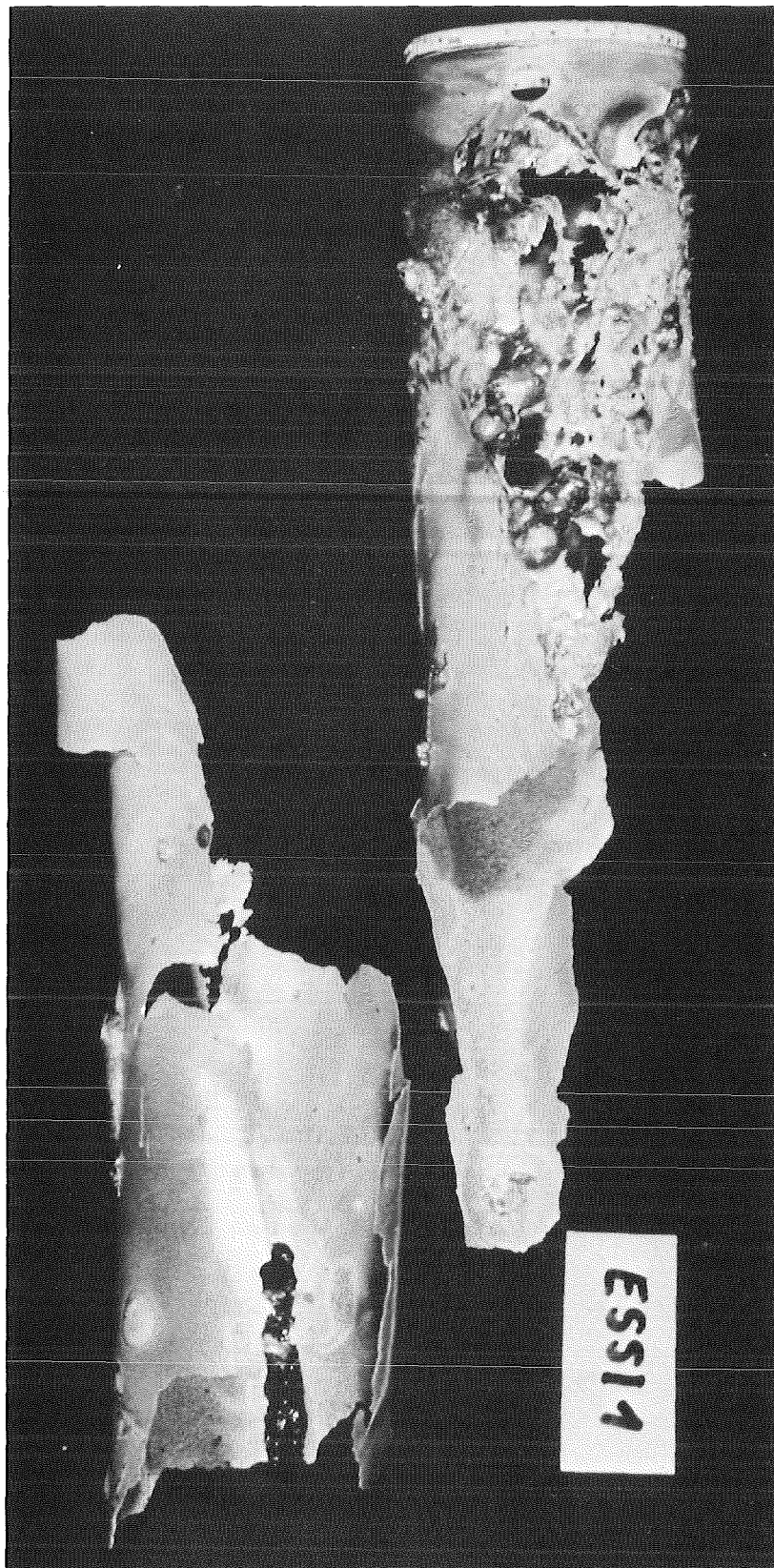


FIG.28: UPPER PART OF SHROUD FROM ESSI-1 AFTER DISMANTLING

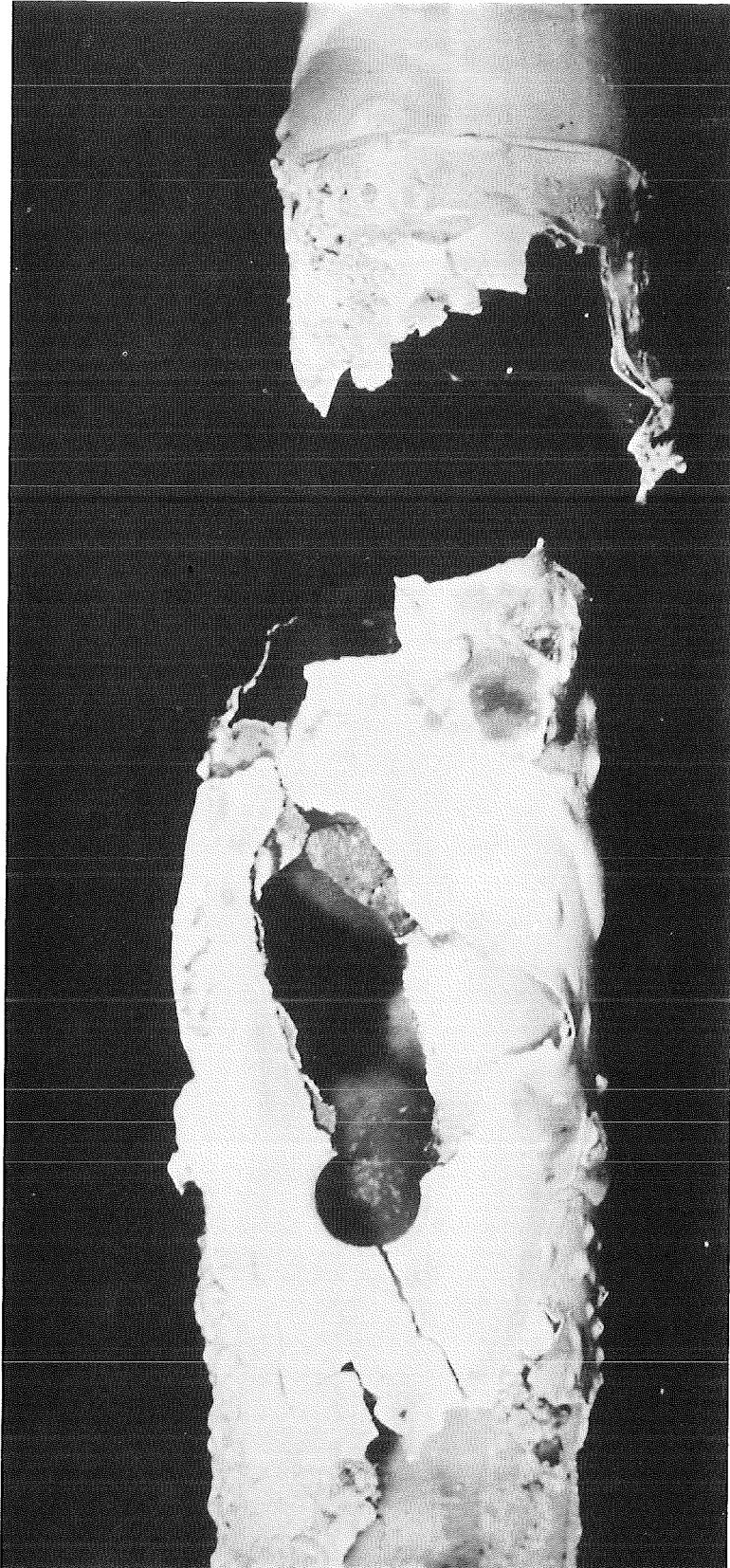


FIG. 29: UPPER PART OF SHROUD FROM ESSI-2 AFTER DISMANTLING

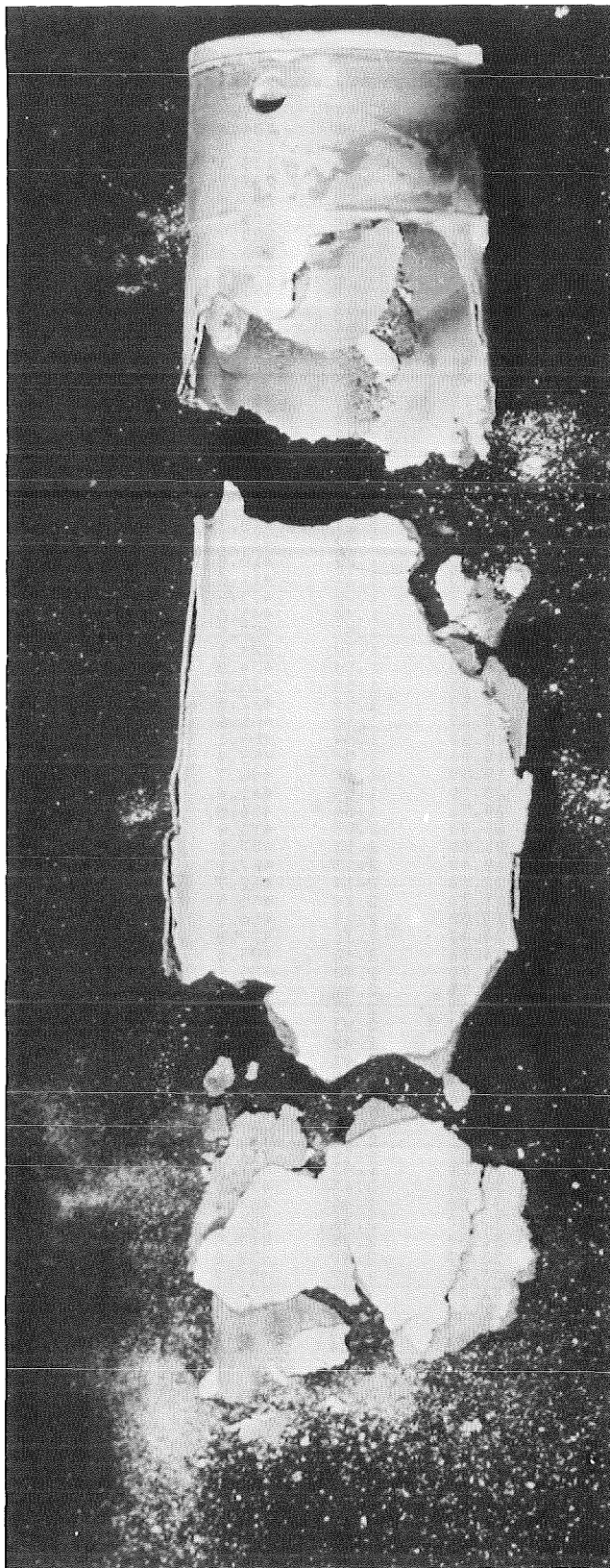


FIG. 30: UPPER PART OF SHROUD FROM ESS1-3 AFTER DISMANTLING

ESSE1	ZEIT [MIN]	U [V]	I [A]	U*I [VA]	U*I [MOM]
	1.00	.00	134.1	.0	.00
	1.50	.00	134.5	.0	.00
	2.00	.00	134.9	.0	.00
	2.50	.00	135.3	.0	.00
	3.00	.28	292.7	83.4	.97
	3.50	.29	289.4	85.0	1.01
	4.00	.30	285.0	84.2	1.04
	4.50	.30	280.7	84.3	1.07
	5.00	.30	276.3	83.8	1.10
	5.50	.31	271.9	83.1	1.12
	6.00	.57	395.9	226.2	1.44
	6.50	.59	378.3	221.7	1.55
	7.00	.60	361.9	215.4	1.64
	7.50	.61	345.7	210.8	1.76
	8.00	.62	331.4	207.0	1.89
	8.50	.63	320.8	202.5	1.97
	9.00	.89	414.0	367.3	2.14
	9.50	.89	395.8	353.9	2.26
	10.00	.90	369.4	331.3	2.43
	10.50	.90	384.2	344.2	2.33
	11.00	.90	379.2	341.2	2.37
	11.50	.90	381.2	343.7	2.37
	12.00	1.16	466.7	543.5	2.47
	12.50	1.21	448.3	541.2	2.69
	13.00	1.22	428.1	520.1	2.84
	13.50	1.22	419.9	511.6	2.90
	14.00	1.22	411.8	502.9	2.97
	14.50	1.22	403.6	494.3	3.03
	15.00	1.48	445.8	657.6	3.31
	15.50	1.53	457.5	700.6	3.75
	16.00	1.54	444.1	682.2	3.46
	16.50	1.54	434.8	668.8	3.54
	17.00	1.54	428.8	659.9	3.59
	17.50	1.54	422.8	651.0	3.64
	18.00	1.78	466.6	830.3	3.81
	18.50	1.84	466.1	855.6	3.94
	19.00	1.84	453.4	832.9	4.05
	19.50	1.84	446.7	821.9	4.12
	20.00	1.84	441.4	812.1	4.17
	20.50	1.84	439.8	808.6	4.18
	21.00	2.03	472.4	959.6	4.30
	21.50	2.13	477.1	1016.5	4.47
	22.00	2.13	467.1	997.0	4.57
	22.50	2.14	462.7	989.3	4.62
	23.00	2.14	458.9	983.0	4.67
	23.50	2.15	458.1	982.9	4.68
	24.00	2.31	477.8	1103.6	4.83
	24.50	2.42	493.0	1192.5	4.91
	25.00	2.42	486.6	1178.2	4.98
	25.50	2.42	480.5	1164.6	5.04
	26.00	2.43	478.8	1161.8	5.07
	26.50	2.43	477.2	1159.0	5.09
	27.00	2.42	476.6	1154.6	5.08
	27.50	2.42	476.8	1156.0	5.09
	28.00	2.43	477.8	1157.8	5.09
	28.50	2.43	477.1	1159.6	5.09
	29.00	2.43	477.3	1161.4	5.10
	29.50	2.43	477.5	1161.5	5.09
	30.00	2.43	477.7	1161.5	5.09
	30.50	2.43	477.9	1161.4	5.09
	31.00	2.43	478.1	1161.3	5.08
	31.50	2.46	484.4	1192.8	5.08
	32.00	2.46	485.2	1193.0	5.07
	32.50	2.46	513.5	1239.5	4.89
	33.00	2.47	439.2	1087.0	5.63
	33.50	2.47	483.7	1192.9	5.10
	34.00	2.45	554.6	1360.9	4.42
	34.50	2.44	580.3	1415.6	4.20
	35.00	2.00	508.8	1015.3	3.92
	35.50	.14	59.2	8.4	2.41



Table 1:  
Voltage, Current, Power and  
Resistance for Test ESS1-1

ESSI2 TIME (MIN)	U (V)	I (A)	U*I (U*A)	U*I (MIOHM)
1.50	.3	258.5	72.4	1.0832
2.00	.5	356.9	189.6	1.4885
2.50	.7	430.8	322.5	1.7376
3.00	1.0	472.1	470.7	2.1119
3.50	1.2	543.3	675.6	2.2884
4.00	1.5	599.0	877.0	2.4444
4.50	1.5	538.1	819.5	2.8297
5.00	1.5	493.6	763.6	3.1337
5.50	1.6	468.8	738.4	3.3604
6.00	1.8	499.7	905.2	3.6250
6.50	2.0	538.2	1091.1	3.7671
7.00	2.1	540.0	1155.5	3.9626
7.50	2.1	513.5	1102.5	4.1818
8.00	2.2	513.3	1105.1	4.1945
8.50	2.2	511.1	1100.4	4.2119
9.00	2.2	509.3	1096.4	4.2266
9.50	2.2	508.7	1096.1	4.2350
10.00	2.2	508.2	1095.7	4.2434
10.50	2.2	509.1	1096.7	4.2316
11.00	2.4	536.1	1283.5	4.4666
11.50	2.6	564.0	1482.2	4.6600
12.00	2.9	581.6	1667.0	4.9280
12.50	3.1	589.1	1840.1	5.3019
13.00	3.4	597.7	2015.0	5.6403
13.50	3.6	606.2	2183.4	5.9412
14.00	3.9	619.9	2386.7	6.2112
14.50	4.0	686.4	2777.6	5.8953
15.00	4.0	661.2	2663.9	6.0930
15.50	4.1	608.1	2466.4	6.6702
16.00	4.1	581.3	2360.5	6.9855
16.50	4.1	573.0	2329.5	7.0946
17.00	4.1	576.0	2344.4	7.0659
17.50	4.1	588.8	2390.0	6.8936
18.00	4.0	599.8	2428.4	6.7502
18.50	1.9	417.4	784.3	4.5016
19.00	.2	65.6	13.2	1.7907
18.03.82				

Table 2:  
Voltage, Current, Power and  
Resistance for Test ESSI-2

ESSI3	ZEIT [MIN]	U [V]	I [A]	U×I [W]	U/I [Ω]
	1.50	.00	120.1	.0	.00
	2.50	.06	177.3	10.9	.35
	3.50	.22	228.4	50.1	.96
	4.50	.26	275.7	72.1	.95
	5.50	.36	317.9	114.4	1.13
	6.50	.45	354.2	160.2	1.28
	7.50	.56	382.5	215.1	1.47
	8.50	.65	406.5	263.6	1.59
	9.50	.74	433.6	319.8	1.70
	10.50	.84	458.6	384.9	1.83
	11.50	.95	465.6	442.1	2.04
	12.50	1.07	468.8	503.1	2.29
	13.50	1.17	475.4	556.3	2.46
	14.50	1.29	484.5	622.7	2.65
	15.50	1.40	493.2	689.0	2.83
	16.50	1.51	501.7	756.3	3.00
	17.50	1.62	510.0	825.3	3.17
	18.50	1.72	518.3	892.0	3.32
	19.50	1.82	531.5	967.2	3.42
	20.50	1.92	532.6	1023.5	3.61
	21.50	2.02	531.8	1075.7	3.80
	22.50	2.12	530.0	1122.4	4.00
	23.50	2.22	533.1	1180.8	4.16
	24.50	2.31	539.1	1246.6	4.29
	25.50	2.42	545.2	1316.7	4.43
	26.50	2.52	552.0	1390.1	4.56
	27.50	2.62	558.8	1464.8	4.69
	28.50	2.72	565.7	1538.5	4.81
	29.50	2.82	573.8	1616.5	4.91
	30.50	2.92	582.0	1697.9	5.01
	31.50	3.02	588.4	1776.2	5.13
	32.50	3.13	593.2	1855.2	5.27
	33.50	3.23	595.8	1923.1	5.42
	34.50	3.33	579.2	1927.2	5.74
	35.50	3.43	588.0	2014.8	5.83
	36.50	3.53	601.5	2122.0	5.86
	37.50	3.63	607.7	2206.9	5.98
	38.50	3.74	613.9	2293.2	6.08
	39.50	3.84	620.1	2383.9	6.20
	40.50	3.96	610.7	2417.3	6.48
	41.50	4.04	597.4	2416.2	6.77
	42.50	4.14	623.7	2584.3	6.64
	43.50	4.24	642.2	2725.5	6.61
	44.50	4.35	656.3	2852.0	6.62
	45.50	4.45	664.6	2955.6	6.69
	46.50	4.48	668.7	2998.6	6.71
	47.50	4.50	666.9	2999.5	6.74
	48.50	4.51	665.2	3000.4	6.78
	49.50	4.49	662.7	2972.6	6.77
	50.50	.46	90.0	41.2	5.09
	51.50	.00	3.4	.0	.00
	52.50	.00	3.1	.0	.00
	53.50	.00	2.8	.0	.00
	54.50	.00	2.5	.0	.00
	55.50	.00	2.2	.0	.00

19.03.82

Table 3:  
Voltage, Current, Power and  
Resistance for Test ESSI-3